ICES REPORT 13-07

April 2013

Goal-oriented model adaptivity for viscous incompressible flows

by

T.M. van Opstal, P.T. Bauman, S. Prudhomme, E.H. van Brummelen

The Institute for Computational Engineering and Sciences
The University of Texas at Austin
Austin, Texas 78712

Reference: T.M. van Opstal, P.T. Bauman, S. Prudhomme, E.H. van Brummelen, Goal-oriented model adaptivity for viscous incompressible flows, ICES REPORT 13-07, The Institute for Computational Engineering and Sciences, The University of Texas at Austin, April 2013.

Goal-oriented model adaptivity for viscous incompressible flows

T.M. van Opstal[a], P.T. Bauman[b], S. Prudhomme[c], E.H. van Brummelen[a]

[a] *MEFD, Eindhoven University of Technology, P.O. Box 513, 5600MB, Eindhoven, Netherlands*
[b] *ICES, The University of Texas at Austin, 201 East 24th St. Stop C0200, Austin, TX 78712, USA*
[c] *Département de Mathématiques et de Génie Industriel, Ecole Polytechnique de Montréal, C.P. 6079, succ. Centre-Ville, Montréal, Québec, Canada H3C 3A7*

Abstract

In this paper, we consider a surrogate model to approximate solutions to steady incompressible Navier-Stokes flow problems. The surrogate model is constructed by replacing the Navier-Stokes model by the Stokes model in some region of the computational domain and by coupling the two models along an interface. The surrogate model creates some approximation error. We propose here an error estimate in terms of quantities of interest and an adaptive strategy to reduce the error by adjusting the position of the interface between the two models. This adaptive modeling framework aims at taking away the burden and heuristics of manually partitioning the domain while providing new insight into the physics. We present several two-dimensional numerical experiments to show that the error estimator is accurate and to demonstrate the efficiency of the adaptive method.

Keywords: Navier-Stokes and Stokes equations, coupling method, model adaptivity, adjoint problem, goal-oriented error estimation

1. Introduction

In many numerical simulations, the mathematical model of choice accurately describes the physical processes but is unfortunately intractable with respect to current computer resources. The idea is then to replace this fine model by a simpler or coarser model in some subregions of the computational domain where it is deemed sufficient. Approximations by means of a surrogate model based on the coupling of multiple models using a domain decomposition-type approach is already quite well established and desirable for several reasons: 1) in the case where the fine model is nonlinear, it may be advantageous to replace it by a linear model to avoid using an iterative solver [10]; 2) in the case that the coarse model can be equivalently recast into a boundary integral formulation, the dimension of the computational domain can simply be reduced by one [5, 31]; 3) finally, in the case of multiscale simulations, one may selectively reduce the number of degrees of freedom by considering a coarse scale model instead of the full fine scale model [1, 20].

Our ultimate interest pertains to airbag inflation simulations. Robust mesh generation and evolution in realistic stowed configuration is very challenging due to the complex geometry. In order to treat this class of problems and circumvent associated issues, two-grid scale models were developed in [29, 30] by approximating the complex flow problem with a linearized boundary integral formulation. The necessary approximations are however not appropriate in the inflated part of the domain and are therefore only used on a subdomain. The sub-grid scale model is then coupled to a more refined fluid model set on the rest of the domain. To explore model-adaptivity in this context, we focus on a simpler model problem that avoids auxiliary complications such as moving domains [28] and time-dependence.

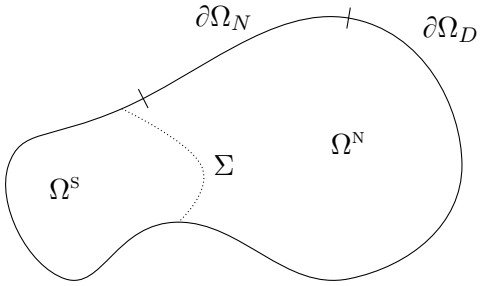

Figure 1: Schematic of domain-decomposition approach for model adaptivity.

A natural question that arises when using an approximate model on a subdomain is, first, which partitions give sufficiently accurate solutions? To define what is actually meant by an accurate solution, one needs to define a measure for accuracy: In many cases, a user has a very restricted interest in the solution, which can be formulated as a functional of the solution, the *goal functional*. In terms of the error in the goal functional, we want to know how large the modeling error is that arises from using an approximate model on a subdomain. Also, we would like to know how to choose this subdomain in an optimal way. Goal-oriented model adaptivity [17, 3, 23] provides a tractable framework in which such questions can be tackled. This framework has been applied to, e.g., heterogeneous materials [18], flow problems [21], atomistic-to-continuum problems [1], free-surface flows [19], turbulence modeling [12] and arterial or river flow [8].

In this work, the Stokes approximation to Navier-Stokes flow is investigated. Earlier work on coupling Navier-Stokes to linearized equations (Oseen, Stokes) was performed by Fatone and co-workers in [9, 10]. However, in the work of Fatone, the subdomain partition is fixed and the modeling error not estimated. This work can be conceived of as an extension of Fatone's work in that direction.

This paper is organized as follows. In Section 2, two formulations for the multiphysics problem are presented. First, in §2.1, a monolithic formulation which is easily implemented; and then, in §2.2, a partitioned formulation which is *a priori* much cheaper. Error estimation and adaptivity is treated in Section 3. In Section 4, first, in §4.1, the discretization and adaptive algorithm are detailed; then, in §4.2-§4.4, the numerical results are presented. We close with a discussion in Section 5.

2. A sharp interface multi-model problem

Consider a bounded, open domain $\Omega \subset \mathbb{R}^2$ with Lipschitz boundary, partitioned into two open subdomains Ω^{N} and Ω^{S} as in figure 1. We will often use the index $m \in \{\mathrm{N}, \mathrm{S}\}$ to denote the Navier-Stokes and Stokes domains, respectively. A partitioning implies $\overline{\Omega^{\mathrm{N}}} \cup \overline{\Omega^{\mathrm{S}}} = \overline{\Omega}$, and $\Omega^{\mathrm{N}} \cap \Omega^{\mathrm{S}} = \varnothing$. We will furthermore assume that Ω^m are also Lipschitz domains so that we can define Sobolev-spaces and their traces on them, as well as their external normals $\boldsymbol{n}^m$ (almost everywhere). The boundary $\partial\Omega$ is partitioned into $\partial\Omega_D$ and $\partial\Omega_N$, along which resp. Dirichlet ($\boldsymbol{g}$) and Neumann data ($\boldsymbol{h}$) are prescribed. In this Section we consider the partitioning, and hence the interface between these subdomains, $\Sigma := \partial\Omega^{\mathrm{N}} - \partial\Omega$, to be predefined. Consider now the steady incompressible

Navier-Stokes equations on Ω^{N} in strong form

$$\boldsymbol{u}^{\mathrm{N}} \cdot \nabla \boldsymbol{u}^{\mathrm{N}} - \nabla \cdot \boldsymbol{\sigma}(\boldsymbol{u}^{\mathrm{N}}, p^{\mathrm{N}}) = \boldsymbol{0} \text{ in } \Omega^{\mathrm{N}}, \tag{1a}$$

$$\nabla \cdot \boldsymbol{u}^{\mathrm{N}} = \boldsymbol{0} \text{ in } \Omega^{\mathrm{N}}, \tag{1b}$$

$$\boldsymbol{u}^{\mathrm{N}} = \boldsymbol{g} \text{ on } \partial\Omega_D \cap \partial\Omega^{\mathrm{N}}, \tag{1c}$$

$$\boldsymbol{\sigma}(\boldsymbol{u}^{\mathrm{N}}, p^{\mathrm{N}}) \cdot \boldsymbol{n}^{\mathrm{N}} = \boldsymbol{h} \text{ on } \partial\Omega_N \cap \partial\Omega^{\mathrm{N}}; \tag{1d}$$

and the Stokes equations on Ω^{S}

$$-\nabla \cdot \boldsymbol{\sigma}(\boldsymbol{u}^{\mathrm{S}}, p^{\mathrm{S}}) = \boldsymbol{0} \text{ in } \Omega^{\mathrm{S}}, \tag{2a}$$

$$\nabla \cdot \boldsymbol{u}^{\mathrm{S}} = \boldsymbol{0} \text{ in } \Omega^{\mathrm{S}}, \tag{2b}$$

$$\boldsymbol{u}^{\mathrm{S}} = \boldsymbol{g} \text{ on } \partial\Omega_D \cap \partial\Omega^{\mathrm{S}}, \tag{2c}$$

$$\boldsymbol{\sigma}(\boldsymbol{u}^{\mathrm{S}}, p^{\mathrm{S}}) \cdot \boldsymbol{n}^{\mathrm{S}} = \boldsymbol{h} \text{ on } \partial\Omega_N \cap \partial\Omega^{\mathrm{S}}; \tag{2d}$$

and suitable transmission conditions on the interface:

$$\boldsymbol{u}^{\mathrm{S}} = \boldsymbol{u}^{\mathrm{N}} \text{ on } \Sigma, \tag{3a}$$

$$\boldsymbol{\sigma}(\boldsymbol{u}^{\mathrm{S}}, p^{\mathrm{S}}) \cdot \boldsymbol{n}^{\mathrm{S}} + \boldsymbol{\sigma}(\boldsymbol{u}^{\mathrm{N}}, p^{\mathrm{N}}) \cdot \boldsymbol{n}^{\mathrm{N}} = 0 \text{ on } \Sigma. \tag{3b}$$

We define the global fields $\boldsymbol{u}$ and p as

$$\boldsymbol{u} := \begin{cases} \boldsymbol{u}^{\mathrm{N}}, & \text{in } \Omega^{\mathrm{N}} \\ \boldsymbol{u}^{\mathrm{S}}, & \text{in } \Omega^{\mathrm{S}} \end{cases}, \quad p := \begin{cases} p^{\mathrm{N}}, & \text{in } \Omega^{\mathrm{N}} \\ p^{\mathrm{S}}, & \text{in } \Omega^{\mathrm{S}} \end{cases},$$

where we leave the definition of $(\boldsymbol{u}, p)$ on Σ undefined for now. The stress is Newtonian, i.e., $\sigma_{ij}(\boldsymbol{u}, p) := -p\delta_{ij} + (u_{i,j} + u_{j,i})/\mathrm{Re}$, with Re the Reynolds number.

2.1. Heterogeneous domain decomposition formulation

We derive a formulation based on [9]. To this end we introduce some notation and define test- and trial spaces. The usual Hilbert Sobolev space with index k is denoted $H^k(\Omega)$, its associated inner product and derived norm are denoted by $(\cdot,\cdot)_{k,\Omega}$ and $\|\cdot\|_{k,\Omega}$, respectively. We identify $H^0(\Omega)$ as $L^2(\Omega)$. The velocity is sought in the space

$$V := \{\boldsymbol{v} \in H^1(\Omega) : \boldsymbol{v} = \boldsymbol{0} \text{ on } \partial\Omega_D\}, \tag{4}$$

equipped with the norm $\|\cdot\|_{1,\Omega}$. We denote by μ and λ Lebesgue volume and surface measures, respectively. For the pressure function space we have

$$Q := \begin{cases} L^2(\Omega), & \lambda(\partial\Omega_N) > 0 \\ \left\{ p \in L^2(\Omega) : \int_\Omega p = 0 \right\}, & \text{otherwise} \end{cases} \tag{5}$$

equipped with the usual norm $\|\cdot\|_{0,\Omega}$. We denote by

$$\gamma^{\partial\Omega} : H^1(\Omega) \to H^{1/2}(\partial\Omega) : \quad \gamma^{\partial\Omega}(\boldsymbol{u}) = \boldsymbol{u} \text{ at } \partial\Omega \tag{6}$$

(in the distributional sense) the standard *trace operator*, and its right inverse, the *lifting operator*, by $\ell^{\partial\Omega} : H^{1/2}(\partial\Omega) \to H^1(\Omega)$. Both exist, and are linear and bounded, see [16]. We will stress they are operators by putting their argument in brackets. We have introduced the notation $H^{1/2}(\partial\Omega)$, it

is simply the range of $\gamma^{\partial\Omega}$ and corresponds to the usual definition of Sobolev spaces with fractional index. We denote the space of bounded linear functionals on $H^{1/2}(\partial\Omega)$ by $H^{-1/2}(\partial\Omega)$. The space $H^{1/2}(\omega)$, with $\omega \subset \partial\Omega$, is the restriction of functions in $H^{1/2}(\partial\Omega)$ to ω. In particular, we have, cf. e.g. [22],

$$H_{00}^{1/2}(\Sigma) := \{\boldsymbol{u} \in H^{1/2}(\Sigma) : \text{the zero extension of } \boldsymbol{u} \text{ to all of } \partial\Omega \text{ is in } H^{1/2}(\partial\Omega)\}. \tag{7}$$

The space $H^{-1/2}(\omega)$ is then defined as the dual space of $H_{00}^{1/2}(\omega)$.

We multiply equations (1-2) by test functions $\boldsymbol{v} \in V$ and $q \in Q$ and integrate by parts to obtain:

$$\begin{aligned}
&\int_{\Omega^{\mathrm{N}}} (\boldsymbol{u}\cdot\nabla\boldsymbol{u})\cdot\boldsymbol{v}\,d\boldsymbol{x} \\
&\quad + \sum_m \left\{ \mathrm{Re}^{-1}\int_{\Omega^m} \nabla\boldsymbol{u} : \nabla\boldsymbol{v}\,d\boldsymbol{x} - \mathrm{Re}^{-1}\oint_{\partial\Omega^m} (\boldsymbol{n}\cdot\nabla\boldsymbol{u})\cdot\boldsymbol{v}\,d\boldsymbol{x} \right. \\
&\quad \left. - \int_{\Omega^m} p\nabla\cdot\boldsymbol{v}\,d\boldsymbol{x} + \oint_{\partial\Omega^m} p\boldsymbol{n}\cdot\boldsymbol{v}\,d\boldsymbol{x} - \int_{\Omega^m} q\nabla\cdot\boldsymbol{u}\,d\boldsymbol{x} \right\} = 0.
\end{aligned}$$

We insert boundary conditions into the boundary integrals, replacing them by

$$\begin{aligned}
&\sum_m \left\{ \oint_{\partial\Omega^m} p\boldsymbol{n}\cdot\boldsymbol{v}\,d\boldsymbol{x} - \mathrm{Re}^{-1}\oint_{\partial\Omega^m} (\boldsymbol{n}\cdot\nabla\boldsymbol{u})\cdot\boldsymbol{v}\,d\boldsymbol{x} \right\} = \\
&\qquad = \sum_m \oint_{\partial\Omega^m} (\boldsymbol{\sigma}\cdot\boldsymbol{n}^m)\cdot\boldsymbol{v}\,d\boldsymbol{x} \\
&\qquad = \int_{\partial\Omega_N} \boldsymbol{h}\cdot\boldsymbol{v}\,d\boldsymbol{x} + \int_\Sigma (\boldsymbol{\sigma}\cdot\boldsymbol{n}^{\mathrm{N}} + \boldsymbol{\sigma}\cdot\boldsymbol{n}^{\mathrm{S}})\cdot\boldsymbol{v}\,d\boldsymbol{x}.
\end{aligned}$$

The latter of the two integrals vanishes for $\boldsymbol{v} \in H^1(\Omega)$ on account of the dynamic transmission condition (3b). We introduce the familiar bi- and trilinear forms

$$a(\boldsymbol{u},\boldsymbol{v}) := \mathrm{Re}^{-1}(\nabla\boldsymbol{u},\nabla\boldsymbol{v})_{0,\Omega}, \tag{8}$$

$$b(\boldsymbol{u},p) := -(\nabla\cdot\boldsymbol{u},p)_{0,\Omega}, \tag{9}$$

$$c(\boldsymbol{u},\boldsymbol{v},\boldsymbol{w}) := (\boldsymbol{u}\cdot\nabla\boldsymbol{v},\boldsymbol{w})_{0,\Omega}, \tag{10}$$

and their restrictions to subdomain m: a^m, b^m, c^m. We arrive at the weak formulation

Given $\boldsymbol{g} \in H^{1/2}(\partial\Omega_D)$, $\boldsymbol{h} \in H^{-1/2}(\partial\Omega_N)$ and a Lipschitz partitioning through Σ, find $(\boldsymbol{u},p) \in (\ell^{\partial\Omega}(\boldsymbol{g}) + V) \times Q$ such that:

$$a(\boldsymbol{u},\boldsymbol{v}) + b(\boldsymbol{v},p) + c^{\mathrm{N}}(\boldsymbol{u},\boldsymbol{u},\boldsymbol{v}) + b(\boldsymbol{u},q) = (\boldsymbol{h},\boldsymbol{v})_{0,\partial\Omega_N} \qquad \forall(\boldsymbol{v},q) \in V \times Q. \tag{11}$$

We introduce the condensed notation

$$\begin{aligned}
\Upsilon &:= \{\boldsymbol{g},\boldsymbol{h}\} \text{ as in (11)} \\
N_\Sigma((\boldsymbol{u},p);(\boldsymbol{v},q)) &:= a(\boldsymbol{u},\boldsymbol{v}) + b(\boldsymbol{v},p) + b(\boldsymbol{u},q) \\
&\qquad + c^{\mathrm{N}}(\boldsymbol{u},\boldsymbol{u},\boldsymbol{v}) \\
F((\boldsymbol{v},q)) &:= (\boldsymbol{h},\boldsymbol{v})_{0,\partial\Omega_N}
\end{aligned}$$

such that (11) is equivalent to

Given Σ *and* Υ*, find* $(\boldsymbol{u}, p) \in V \times Q$ *such that:*

$$N_\Sigma((\boldsymbol{u}, p); (\boldsymbol{v}, q)) = F((\boldsymbol{v}, q)) \qquad \forall (\boldsymbol{v}, q) \in V \times Q \tag{12}$$

Remark. We thus find that on the interface Σ, the kinematic condition (3a) is imposed strongly through (4). The dynamic condition (3b) is imposed weakly, and in a variationally consistent way [26] through those test functions $\boldsymbol{v}$ which are supported on Σ.

Remark. Proving the well-posedness of the the system (12), is not trivial and beyond the scope of this article. Use of the skew-symmetric form of the convective term $c^{\mathrm{N}}(\cdot,\cdot,\cdot)$ facilitates such a result. Considering the homogeneous Dirichlet case, any $\boldsymbol{v} \in V$ and a (weakly) solenoidal vector field $\boldsymbol{u}^{\mathrm{N}} \in V$ (any solution $\boldsymbol{u}^{\mathrm{N}}$ of (12) will satisfy this condition), we have (see e.g. [11, 15, 25]) the identity

$$c^{\mathrm{N}}(\boldsymbol{u}^{\mathrm{N}}, \boldsymbol{u}^{\mathrm{N}}, \boldsymbol{v}) = -c^{\mathrm{N}}(\boldsymbol{u}^{\mathrm{N}}, \boldsymbol{v}, \boldsymbol{u}^{\mathrm{N}}) + \int_\Sigma (\boldsymbol{u}^{\mathrm{N}} \cdot \boldsymbol{v})(\boldsymbol{u}^{\mathrm{N}} \cdot \boldsymbol{n}^{\mathrm{N}}) d\boldsymbol{x}.$$

This property motivates the introduction of the skew-symmetric convection term

$$d^{\mathrm{N}}(\boldsymbol{u}, \boldsymbol{v}, \boldsymbol{w}) = \frac{1}{2} c^{\mathrm{N}}(\boldsymbol{u}, \boldsymbol{v}, \boldsymbol{w}) - \frac{1}{2} c^{\mathrm{N}}(\boldsymbol{u}, \boldsymbol{w}, \boldsymbol{v}) \tag{13}$$

and the reformulation of the transmission condition (3b), equating the *Oseen fluxes* along the interface:

$$\boldsymbol{\sigma}(\boldsymbol{u}^{\mathrm{S}}, p^{\mathrm{S}}) \cdot \boldsymbol{n}^{\mathrm{S}} + \left(\boldsymbol{\sigma}(\boldsymbol{u}^{\mathrm{N}}, p^{\mathrm{N}}) - \frac{1}{2} \boldsymbol{u}^{\mathrm{N}} \otimes \boldsymbol{u}^{\mathrm{N}} \right) \cdot \boldsymbol{n}^{\mathrm{N}} = 0 \qquad \text{on } \Sigma, \tag{14}$$

yielding a formulation for which an existence and uniqueness result is known, this is the main result of [10], theorem 6.1. In the sequel, however, we will work with the standard dynamic condition (3b) and convective term (10). A comparison between the choices (3b) and (14) is given in [9].

2.2. Partitioned iterative scheme

An alternative approach to the problem (1-3), is to treat the two subdomains, Ω^{N} and Ω^{S}, separately, and to iterate the coupled formulation until convergence. Then a choice has to be made in the enforcement of the transmission conditions (3). This results in a partitioned solution approach, which gives a user the freedom to select specialized solvers for each subproblem. In this setting, for instance, a Galerkin discretization of the Stokes problem typically gives a linear, symmetric matrix. Alternatively, as demonstrated in [30], a treatment of the Stokes problem by the boundary element method would enable flow calculations on highly complex, evolving domains. In this Section, we present a partitioned formulation, and show its equivalence to the monolithic formulation (12).

We consider only the multi-model case $\mu(\Omega^m) > 0$. The homogeneous cases have been treated in e.g. [11, 15, 25]. The choice of a partitioned formulation includes a particular imposition of interface conditions, and for a well-posed iterative scheme this depends on the presence of a Neumann boundary and on the domain partition it falls into. For convenient definitions of the function spaces in (15-16), we consider here only the case that the subdomains Ω^m are connected and that the Neumann boundary is entirely encapsulated within the Navier-Stokes partition, but the analysis extends with minor modifications to other configurations. The relevant function spaces are

$$V^m := \{\boldsymbol{v} \in H^1(\Omega) : \ \boldsymbol{v} = \boldsymbol{0} \text{ on } \Omega - \Omega^m, \ \boldsymbol{v} = \boldsymbol{0} \text{ on } \partial\Omega_D\}, \tag{15}$$

$$Q^m := \{p \in L^2(\Omega) : \ p = 0 \text{ on } \Omega - \Omega^m\}, \tag{16a}$$

and in the case $\lambda(\partial\Omega_N) = 0$,

$$Q^{\mathrm{N}} := \left\{ p^{\mathrm{N}} \in L^2(\Omega) : \; p^{\mathrm{N}} = 0 \text{ on } \Omega^{\mathrm{S}}, \; \int_{\Omega^{\mathrm{N}}} p^{\mathrm{N}} = -\int_{\Omega^{\mathrm{S}}} p^{\mathrm{S}} \right\}. \tag{16b}$$

The space Q^{S} requires no modifications, the Neumann boundary Σ has positive measure, such that the (mean) pressure in the Stokes subproblem is uniquely determined. For the same reason, we ignore the case where Ω^{N} is not connected and one of the closed boundary segments does not contain such a Neumann boundary of positive measure. Throughout this Section we use the notations $\boldsymbol{u}^m$ and p^m, $m \in \{\mathrm{N}, \mathrm{S}\}$, but these do not denote the classic solution of Section 2. Rather, we denote by them elements of the spaces V^m and Q^m.

For the purpose of discussion, let us restrict ourselves to the case where the interface is away from the Neumann boundary, i.e. $\operatorname{dist}(\Sigma, \partial\Omega_N) > 0$. There is a trace operator $\gamma^\Sigma : V \to H^{1/2}_{00}(\Sigma)$ (choosing Ω as Ω^{N} in equation 7), such that $\gamma^\Sigma(\boldsymbol{v}) = \boldsymbol{v}$ on Σ. In the case that Σ is a closed contour we simply have $\gamma^\Sigma : V \to H^{1/2}(\Sigma)$. We define a lifting operator $\ell^\Sigma : H^{1/2}_{00}(\Sigma) \to V$, a right inverse of γ^Σ. Then, we have the splitting

Lemma 1. *$V = V^{\mathrm{N}} \oplus \ell^\Sigma H^{1/2}_{00}(\Sigma) \oplus V^{\mathrm{S}}$, $Q = Q^{\mathrm{N}} \oplus Q^{\mathrm{S}}$.*

Corollary 2. *There exists $\forall (\boldsymbol{v}, q) \in V \times Q$ and $\forall \boldsymbol{x} \in \Omega^m$ a splitting (which we actually construct in the proof of lemma 1)*

$$\begin{aligned} \boldsymbol{v} &= \boldsymbol{v}^{\mathrm{N}} + \ell^\Sigma(\boldsymbol{v}^{00}) + \boldsymbol{v}^{\mathrm{S}} \\ q &= q^{\mathrm{N}} + q^{\mathrm{S}} \end{aligned} \tag{17}$$

with $\boldsymbol{v}^m \in V^m$; $\boldsymbol{v}^{00} \in H^{1/2}_{00}(\Sigma)$ and $q^m \in Q^m$ for $m \in \{\mathrm{N}, \mathrm{S}\}$. Conversely, any such combination of $\boldsymbol{v}^m$ and $\ell^\Sigma(\boldsymbol{v}^{00})$ yields an element $\boldsymbol{v}$ in V, and any combination q^m yields an element $q \in Q$.

Proof. (of lemma 1) The forward inclusion, "$\supset$", of the first equality is straightforward. Note that V is a vector space, so we prove the separate conclusions. $V \supset V^m$ is readily seen from the definitions (4) and (15), and $V \supset \ell^\Sigma H^{1/2}_{00}(\Sigma)$ follows from the range of $\ell^\Sigma(\cdot)$.

For the backward inclusion, "$\subset$", note that $\tilde{\boldsymbol{v}} := \boldsymbol{v} - \ell^\Sigma(\boldsymbol{v}^{00}) = \boldsymbol{0}$ on Σ by the definition of ℓ^Σ. Then $\boldsymbol{v}^m := \tilde{\boldsymbol{v}}|_{\Omega^m} \in V^m$, such that the first of (17) holds.

For the second equality we simply define $q^m = q|_{\Omega^m}$ which is clearly an element of Q^m. Noting that $Q = \left\{ q \in L^2(\Omega) : q|_{\Omega^m} \in Q^m \right\}$, by comparing equations (5) and (16) we also have $Q^m \subset Q$.

Motivated by the splitting provided by (17), we directly cast the monolithic formulation (11) into the partitioned scheme below. Introducing the functionals

$$\begin{aligned} N^{\mathrm{N}}_k((\boldsymbol{u}^{\mathrm{N}}, p^{\mathrm{N}}); (\boldsymbol{v}^{\mathrm{N}}, q^{\mathrm{N}})) &:= a^{\mathrm{N}}(\boldsymbol{u}^{\mathrm{N}}, \boldsymbol{v}^{\mathrm{N}}) + b^{\mathrm{N}}(\boldsymbol{v}^{\mathrm{N}}, p^{\mathrm{N}}) + c^{\mathrm{N}}(\boldsymbol{u}^{\mathrm{N}}, \boldsymbol{u}^{\mathrm{N}}, \boldsymbol{v}^{\mathrm{N}}) \\ &\quad + c^{\mathrm{N}}\big(\boldsymbol{u}^{\mathrm{N}}, \ell^\Sigma(\boldsymbol{u}^{00}_{k-1}), \boldsymbol{v}^{\mathrm{N}}\big) + c^{\mathrm{N}}\big(\ell^\Sigma(\boldsymbol{u}^{00}_{k-1}), \boldsymbol{u}^{\mathrm{N}}, \boldsymbol{v}^{\mathrm{N}}\big) + b^{\mathrm{N}}(\boldsymbol{u}^{\mathrm{N}}, q^{\mathrm{N}}), \\ F^{\mathrm{N}}_k((\boldsymbol{v}^{\mathrm{N}}, q^{\mathrm{N}})) &:= (\boldsymbol{h}, \boldsymbol{v}^{\mathrm{N}})_{0,\partial\Omega_N} - a^{\mathrm{N}}\big(\ell^\Sigma(\boldsymbol{u}^{00}_{k-1}), \boldsymbol{v}^{\mathrm{N}}\big) - b^{\mathrm{N}}\big(\ell^\Sigma(\boldsymbol{u}^{00}_{k-1}), q^{\mathrm{N}}\big) \\ &\quad - c^{\mathrm{N}}\big(\ell^\Sigma(\boldsymbol{u}^{00}_{k-1}), \ell^\Sigma(\boldsymbol{u}^{00}_{k-1}), \boldsymbol{v}^{\mathrm{N}}\big), \end{aligned}$$

and[1]

$$
\begin{aligned}
N_k^{\mathrm{S}}\big((\boldsymbol{u}^{\mathrm{S}},p^{\mathrm{S}},\boldsymbol{u}^{00}),(\boldsymbol{v}^{\mathrm{S}},p^{\mathrm{S}},\boldsymbol{v}^{00})\big) &:= a\big(\boldsymbol{u}^{\mathrm{S}}+\ell^{\Sigma}(\boldsymbol{u}^{00}),\boldsymbol{v}^{\mathrm{S}}+\ell^{\Sigma}(\boldsymbol{v}^{00})\big)\\
&+ b^{\mathrm{S}}\big(\boldsymbol{v}^{\mathrm{S}}+\ell^{\Sigma}(\boldsymbol{v}^{00}),p^{\mathrm{S}}\big)+c^{\mathrm{N}}\big(\ell^{\Sigma}(\boldsymbol{u}^{00}),\boldsymbol{u}^{\mathrm{N}},\ell^{\Sigma}(\boldsymbol{v}^{00})\big)\\
&+ c^{\mathrm{N}}\big(\boldsymbol{u}^{\mathrm{N}}+\ell^{\Sigma}(\boldsymbol{u}_{k-1}^{00}),\ell^{\Sigma}(\boldsymbol{u}^{00}),\ell^{\Sigma}(\boldsymbol{v}^{00})\big)+b^{\mathrm{S}}\big(\boldsymbol{u}^{\mathrm{S}}+\ell^{\Sigma}(\boldsymbol{u}^{00}),q^{\mathrm{S}}\big),\\
F_k^{\mathrm{S}}\big((\boldsymbol{v}^{\mathrm{S}},q^{\mathrm{S}},\boldsymbol{v}^{00})\big) &:= \big(\boldsymbol{h},\ell^{\Sigma}(\boldsymbol{v}^{00})\big)_{0,\partial\Omega_N}-a^{\mathrm{N}}\big(\boldsymbol{u}^{\mathrm{N}},\ell^{\Sigma}(\boldsymbol{v}^{00})\big)-c^{\mathrm{N}}\big(\boldsymbol{u}^{\mathrm{N}},\boldsymbol{u}^{\mathrm{N}},\ell^{\Sigma}(\boldsymbol{v}^{00})\big)\\
&- b^{\mathrm{N}}\big(\ell^{\Sigma}(\boldsymbol{v}^{00}),p^{\mathrm{N}}\big),
\end{aligned}
$$

we have the following partitioned scheme.

Given the input $\boldsymbol{g}\in H^{1/2}(\partial\Omega_D)$ and $\boldsymbol{h}\in H^{-1/2}(\partial\Omega_N)$ and initial guess(es) $\boldsymbol{u}_0^{00}\in H_{00}^{1/2}(\Sigma)$, and, in the case of equation (16b), $p^{\mathrm{S}}\in Q^{\mathrm{S}}$ we solve for $k\in\mathbb{N}$

Find $(\boldsymbol{u}_k^{\mathrm{N}},p_k^{\mathrm{N}})\in(\ell^{\partial\Omega_D}(\boldsymbol{g})+V^{\mathrm{N}})\times Q^{\mathrm{N}}$ *such that:*

$$
N_k^{\mathrm{N}}\left((\boldsymbol{u}_k^{\mathrm{N}},p_k^{\mathrm{N}});(\boldsymbol{v}^{\mathrm{N}},q^{\mathrm{N}})\right)=F_k^{\mathrm{N}}\left((\boldsymbol{v}^{\mathrm{N}},q^{\mathrm{N}})\right)\qquad\forall(\boldsymbol{v}^{\mathrm{N}},q^{\mathrm{N}})\in V^{\mathrm{N}}\times Q^{\mathrm{N}},\tag{18a}
$$

and subsequently, given $\boldsymbol{u}_k^{\mathrm{N}}$,

Find $(\boldsymbol{u}_k^{\mathrm{S}},p_k^{\mathrm{S}},\boldsymbol{u}_k^{00})\in(\ell^{\partial\Omega_D}(\boldsymbol{g})+V^{\mathrm{S}})\times Q^{\mathrm{S}}\times H_{00}^{1/2}(\Sigma)$ *such that:*

$$
\begin{aligned}
N_k^{\mathrm{S}}\left((\boldsymbol{u}_k^{\mathrm{S}},p_k^{\mathrm{S}},\boldsymbol{u}_k^{00}),(\boldsymbol{v}^{\mathrm{S}},p^{\mathrm{S}},\boldsymbol{v}^{00})\right)&=F_k^{\mathrm{S}}\left((\boldsymbol{v}^{\mathrm{S}},q^{\mathrm{S}},\boldsymbol{v}^{00})\right)\\
&\forall(\boldsymbol{v}^{\mathrm{S}},q^{\mathrm{S}},\boldsymbol{v}^{00})\in V^{\mathrm{S}}\times Q^{\mathrm{S}}\times H_{00}^{1/2}(\Sigma),
\end{aligned}\tag{18b}
$$

and returning to (18a) with, for some $\vartheta\in(0,1]$,

$$
(\boldsymbol{u}_k^m,p_k^m)\leftarrow\vartheta(\boldsymbol{u}_k^m,p_k^m)+(1-\vartheta)(\boldsymbol{u}_{k-1}^m,p_{k-1}^m)\tag{18c}
$$

and $k\leftarrow k+1$.

In summary, the kinematic condition (3a) is imposed strongly in the Navier-Stokes subproblem (18a). The dynamic condition (3b) is imposed weakly in the linear Stokes subproblem (18b), by evaluating the residual $F_k^{\mathrm{N}}(\cdot)-N_k^{\mathrm{N}}((\boldsymbol{u}^{\mathrm{N}},p^{\mathrm{N}}),\cdot)$ against functions $(\ell^{\Sigma}(\boldsymbol{v}^{00}),\cdot)$.

Theorem 3. *The problems (11) (or its compact notation (12)) and (18) are equivalent, in the sense that* $(\boldsymbol{u},p)$ *is the solution of (11) if and only if its splitting through lemma 1,* $(\boldsymbol{u}^{\mathrm{N}},\boldsymbol{u}^{\mathrm{S}},\boldsymbol{u}^{00},p^{\mathrm{N}},p^{\mathrm{S}})$*, is the limit solution of (18), i.e.,*

$$
\begin{aligned}
\boldsymbol{u}^m&=\lim_{k\to\infty}\boldsymbol{u}_k^m\in V^m,\\
\boldsymbol{u}^{00}&=\lim_{k\to\infty}\boldsymbol{u}_k^{00}\in H_{00}^{1/2}(\Sigma),\\
p^m&=\lim_{k\to\infty}p_k^m\in Q^m,
\end{aligned}
$$

where the limits reside in the trial spaces by completeness. The partitioned scheme is assumed to converge as $k\to\infty$*.*

[1] If indeed $\operatorname{dist}(\Sigma,\partial\Omega_N)>0$, and the implemented lift ℓ^{Σ} maps to functions with local support, away from $\partial\Omega_N$, the first term in the last functional, F_k^{s}, may drop. This is quite common in implementation.

Proof. For the forward implication, $\Rightarrow$, invoke lemma 1 to substitute the splitting (17), into (11) for both test and trial functions. Using the abridged notation $\boldsymbol{f}^{\Sigma} := \ell^{\Sigma}(\boldsymbol{f}^{00})$ and $\boldsymbol{f}^{\partial\Omega} := \ell^{\partial\Omega}(\boldsymbol{f})$ yields, for each of the terms in (11),

$$
\begin{aligned}
a(\boldsymbol{u}^{\mathrm{N}} + \boldsymbol{u}^{\mathrm{S}} + \boldsymbol{u}^{\Sigma}, \boldsymbol{v}^{\mathrm{N}} + \boldsymbol{v}^{\mathrm{S}} + \boldsymbol{v}^{\Sigma}) &= \underbrace{a^{\mathrm{N}}(\boldsymbol{u}^{\mathrm{N}}, \boldsymbol{v}^{\mathrm{N}}) + a^{\mathrm{N}}(\boldsymbol{u}^{\Sigma}, \boldsymbol{v}^{\mathrm{N}})}_{\text{(a)}} + \\
&+ \underbrace{a^{\mathrm{N}}(\boldsymbol{u}^{\mathrm{N}}, \boldsymbol{v}^{\Sigma}) + a^{\mathrm{S}}(\boldsymbol{u}^{\mathrm{S}}, \boldsymbol{v}^{\mathrm{S}}) + a^{\mathrm{S}}(\boldsymbol{u}^{\mathrm{S}}, \boldsymbol{v}^{\Sigma}) + a^{\mathrm{S}}(\boldsymbol{u}^{\Sigma}, \boldsymbol{v}^{\mathrm{S}}) + a(\boldsymbol{u}^{\Sigma}, \boldsymbol{v}^{\Sigma})}_{\text{(b)}}, \\
b(\boldsymbol{u}^{\mathrm{N}} + \boldsymbol{u}^{\mathrm{S}} + \boldsymbol{u}^{\Sigma}, q^{\mathrm{N}} + q^{\mathrm{S}}) &= \underbrace{b^{\mathrm{N}}(\boldsymbol{u}^{\mathrm{N}}, q^{\mathrm{N}}) + b^{\mathrm{N}}(\boldsymbol{u}^{\Sigma}, q^{\mathrm{N}})}_{\text{(a)}} + \underbrace{b^{\mathrm{S}}(\boldsymbol{u}^{\mathrm{S}}, q^{\mathrm{S}}) + b^{\mathrm{S}}(\boldsymbol{u}^{\Sigma}, q^{\mathrm{S}})}_{\text{(b)}}, \\
b(\boldsymbol{v}^{\mathrm{N}} + \boldsymbol{v}^{\mathrm{S}} + \boldsymbol{v}^{\Sigma}, p^{\mathrm{N}} + p^{\mathrm{S}}) &= \underbrace{b^{\mathrm{N}}(\boldsymbol{v}^{\mathrm{N}}, p^{\mathrm{N}})}_{\text{(a)}} + \underbrace{b^{\mathrm{N}}(\boldsymbol{v}^{\Sigma}, p^{\mathrm{N}}) + b^{\mathrm{S}}(\boldsymbol{v}^{\mathrm{S}}, p^{\mathrm{S}}) + b^{\mathrm{S}}(\boldsymbol{v}^{\Sigma}, p^{\mathrm{S}})}_{\text{(b)}}, \\
c^{\mathrm{N}}(\boldsymbol{u}^{\mathrm{N}} + \boldsymbol{u}^{\mathrm{S}} + \boldsymbol{u}^{\Sigma} + \boldsymbol{g}^{\partial\Omega}, \boldsymbol{u}^{\mathrm{N}} + \boldsymbol{u}^{\mathrm{S}} + \boldsymbol{u}^{\Sigma} + \boldsymbol{g}^{\partial\Omega}, \boldsymbol{v}^{\mathrm{N}} + \boldsymbol{v}^{\mathrm{S}} + \boldsymbol{v}^{\Sigma}) &= \\
&= \underbrace{c^{\mathrm{N}}(\boldsymbol{u}^{\mathrm{N}}, \boldsymbol{u}^{\mathrm{N}}, \boldsymbol{v}^{\mathrm{N}}) + c^{\mathrm{N}}(\boldsymbol{u}^{\mathrm{N}}, \boldsymbol{u}^{\Sigma} + \boldsymbol{g}^{\partial\Omega}, \boldsymbol{v}^{\mathrm{N}}) + c^{\mathrm{N}}(\boldsymbol{u}^{\Sigma} + \boldsymbol{g}^{\partial\Omega}, \boldsymbol{u}^{\mathrm{N}}, \boldsymbol{v}^{\mathrm{N}})}_{\text{(a)}} + \\
&+ \underbrace{c^{\mathrm{N}}(\boldsymbol{u}^{\Sigma} + \boldsymbol{g}^{\partial\Omega}, \boldsymbol{u}^{\Sigma} + \boldsymbol{g}^{\partial\Omega}, \boldsymbol{v}^{\mathrm{N}})}_{\text{(a)}} + \underbrace{c^{\mathrm{N}}(\boldsymbol{u}^{\mathrm{N}} + \boldsymbol{g}^{\partial\Omega}, \boldsymbol{u}^{\mathrm{N}} + \boldsymbol{g}^{\partial\Omega}, \boldsymbol{v}^{\Sigma})}_{\text{(b)}} + \\
&+ \underbrace{c^{\mathrm{N}}(\boldsymbol{u}^{\mathrm{N}} + \boldsymbol{g}^{\partial\Omega}, \boldsymbol{u}^{\Sigma}, \boldsymbol{v}^{\Sigma}) + c^{\mathrm{N}}(\boldsymbol{u}^{\Sigma}, \boldsymbol{u}^{\mathrm{N}} + \boldsymbol{g}^{\partial\Omega}, \boldsymbol{v}^{\Sigma}) + c^{\mathrm{N}}(\boldsymbol{u}^{\Sigma}, \boldsymbol{u}^{\Sigma}, \boldsymbol{v}^{\Sigma})}_{\text{(b)}}, \\
(\boldsymbol{h}, \boldsymbol{v}^{\mathrm{N}} + \boldsymbol{v}^{\mathrm{S}} + \boldsymbol{v}^{\Sigma})_{0,\partial\Omega_N} &= \underbrace{(\boldsymbol{h}, \boldsymbol{v}^{\mathrm{N}})_{0,\partial\Omega_N}}_{\text{(a)}} + \underbrace{(\boldsymbol{h}, \boldsymbol{v}^{\Sigma})_{0,\partial\Omega_N}}_{\text{(b)}}, \\
a(\boldsymbol{g}^{\partial\Omega}, \boldsymbol{v}^{\mathrm{N}} + \boldsymbol{v}^{\mathrm{S}} + \boldsymbol{v}^{\Sigma}) &= \underbrace{a^{\mathrm{N}}(\boldsymbol{g}^{\partial\Omega}, \boldsymbol{v}^{\mathrm{N}})}_{\text{(a)}} + \underbrace{a(\boldsymbol{g}^{\partial\Omega}, \boldsymbol{v}^{\Sigma}) + a^{\mathrm{S}}(\boldsymbol{g}^{\partial\Omega}, \boldsymbol{v}^{\mathrm{S}})}_{\text{(b)}}, \\
b(\boldsymbol{g}^{\partial\Omega}, q^{\mathrm{N}} + q^{\mathrm{S}}) &= \underbrace{b^{\mathrm{N}}(\boldsymbol{g}^{\partial\Omega}, q^{\mathrm{N}})}_{\text{(a)}} + \underbrace{b^{\mathrm{S}}(\boldsymbol{g}^{\partial\Omega}, q^{\mathrm{S}})}_{\text{(b)}}.
\end{aligned}
$$

We sum the terms (a), i.e. those tested against $(\boldsymbol{v}^{\mathrm{N}}, q^{\mathrm{N}})$, and observe that these correspond to (18a). Conversely, terms (b) correspond to (18b). Thus, the solution $(\boldsymbol{u}, p)$ of (11) is a fixed point of the partitioned iteration (18).

Conversely, for the reverse implication $\Leftarrow$, if $(\boldsymbol{u}^{\mathrm{N}}, \boldsymbol{u}^{\mathrm{S}}, \boldsymbol{u}^{00}, p^{\mathrm{N}}, p^{\mathrm{S}})$ is the limit of the partitioned process (18), the summation of equations (18a-18b) is equivalent to the monolithic formulation (11), by virtue of the same splitting.

3. A posteriori error estimation and adaptivity

In this Section, we shall consider that one is interested, not in the solution $(\boldsymbol{u}, p)$ of (12), but in the prediction of some (differentiable) functional of the solution $J((\boldsymbol{u}, p))$, the *goal quantity*, for example:

1. the vorticity in subregion $\omega \subset \mathbb{R}^2$ (e.g. in lower right corner of the cavity, in Figure 2 on page 14):

$$J((\boldsymbol{u}, p)) = \int_{\omega} \operatorname{curl} \boldsymbol{u} = \int_{\omega} u_{0,1} - u_{1,0} \tag{19}$$

2. the $\boldsymbol{v}$-weighted traction $\boldsymbol{\sigma} \cdot \boldsymbol{n}$, for some $\boldsymbol{v} \in H^{1/2}(\partial\Omega)$:[2]

$$\begin{aligned} J((\boldsymbol{u},p)) &= \oint_{\partial\Omega} (\boldsymbol{\sigma}(\boldsymbol{u},p)\cdot\boldsymbol{n})\cdot\boldsymbol{v} \\ &= F((\ell^{\partial\Omega}(\boldsymbol{v}),0)) - N_\Sigma((\boldsymbol{u},p),(\ell^{\partial\Omega}(\boldsymbol{v}),0)), \end{aligned}$$

   with $\gamma^{\partial\Omega}$ as in (6), where the last equality follows by interpreting the boundary integral as a $H^{-1/2}(\partial\Omega) \times H^{1/2}(\Omega)$ duality pairing such that the functional is bounded.

3. kinetic energy (nonlinear goal):

$$J((\boldsymbol{u},p)) = \frac{1}{2}\|\boldsymbol{u}\|_{0,\Omega}^2$$

4. average or mollified versions of pointwise values, as in [21].

In general, it may not be necessary to solve the Navier-Stokes equations on the whole domain Ω to achieve an acceptable accuracy in the goal quantity, and it may suffice to use an approximation, the Stokes equations, on a subdomain (when the convective term is small with respect to the diffusive term, for example). Goal oriented model adaptivity provides a systematic way to arrive at an optimal discretization. In this Section we present the methodology, based on [17, 21], beginning with the introduction of some notation.

Fréchet derivatives of nonlinear operators $J(\cdot)$ and semilinear operators $N(\cdot;\cdot)$ are defined as, $\forall \boldsymbol{u} \in H^1(\Omega)$; $\forall \boldsymbol{v}, \boldsymbol{w}, \boldsymbol{x} \in V$ and $\forall p, q, r, s \in Q$,

$$\begin{aligned} &J'((\boldsymbol{u},p);(\boldsymbol{v},q)) = \\ &\quad \lim_{t\to 0} t^{-1}\left[J((\boldsymbol{u}+t\boldsymbol{v},p+tq)) - J((\boldsymbol{u},p))\right] \\ &J''((\boldsymbol{u},p);(\boldsymbol{v},q),(\boldsymbol{w},r)) = \\ &\quad \lim_{t\to 0} t^{-1}\left[J'((\boldsymbol{u}+t\boldsymbol{w},p+tr);(\boldsymbol{v},q)) - J'((\boldsymbol{u},p);(\boldsymbol{v},q))\right] \end{aligned}$$

and

$$\begin{aligned} &N'((\boldsymbol{u},p);(\boldsymbol{v},q),(\boldsymbol{w},r)) = \\ &\quad \lim_{t\to 0} t^{-1}\left[N((\boldsymbol{u}+t\boldsymbol{w},p+tr);(\boldsymbol{v},q)) - N((\boldsymbol{u},p);(\boldsymbol{v},q))\right] \\ &N''((\boldsymbol{u},p);(\boldsymbol{v},q),(\boldsymbol{w},r),(\boldsymbol{x},s)) = \\ &\quad \lim_{t\to 0} t^{-1}\left[N((\boldsymbol{u}+t\boldsymbol{x},p+ts);(\boldsymbol{v},q),(\boldsymbol{w},r)) - N((\boldsymbol{u},p);(\boldsymbol{v},q),(\boldsymbol{w},r))\right] \end{aligned}$$

provided the existence of the limits.

Now consider the nonlinear *fine* model (where Υ denotes the data, as in equation 12)

Given Σ_1 *and* Υ*, find* $(\boldsymbol{u}_1,p_1) \in (\ell^{\partial\Omega_D}(\boldsymbol{g}) + V) \times Q$ *such that:*

$$N_{\Sigma_1}((\boldsymbol{u}_1,p_1);(\boldsymbol{v},q)) = F((\boldsymbol{v},q)) \quad \forall (\boldsymbol{v},q) \in V \times Q, \tag{20}$$

where Σ_1 is such that $\Omega^{\mathrm{N}} = \Omega$ and hence $\Omega^{\mathrm{S}} = \varnothing$. The residual at an approximation $(\boldsymbol{u}_0,p_0)$ is given by

$$\mathcal{R}((\boldsymbol{u}_0,p_0);(\boldsymbol{v},q)) := F((\boldsymbol{v},q)) - N_{\Sigma_1}((\boldsymbol{u}_0,p_0);(\boldsymbol{v},q)). \tag{21}$$

[2]This is similar to a residual evaluation at a function with support on (part of) $\partial\Omega_D$, see also [26].

We solve an approximate mixed-model problem

Given Σ_0 *and* Υ*, find* $(\boldsymbol{u}_0, p_0) \in (\ell^{\partial\Omega_D}(\boldsymbol{g}) + V) \times Q$ *such that:*

$$N_{\Sigma_0}((\boldsymbol{u}_0, p_0); (\boldsymbol{v}, q)) = F((\boldsymbol{v}, q)) \quad \forall (\boldsymbol{v}, q) \in V \times Q. \tag{22}$$

We can find the dual (or adjoint) solution, related to (20) and the the goal quantity J through the dual (adjoint) problem

Given Σ_1*, find* $(\boldsymbol{z}, \zeta) \in V \times Q$ *such that:*

$$N'_{\Sigma_1}((\boldsymbol{u}_0, p_0); (\boldsymbol{v}, q), (\boldsymbol{z}, \zeta)) = J'((\boldsymbol{u}_0, p_0); (\boldsymbol{v}, q)) \quad \forall (\boldsymbol{v}, q) \in V \times Q \tag{23}$$

In the case that this problem is too expensive to solve, one can also approximate the dual solution by solving the adjoint equation of the forward problem (22) as explained in [3, 27]. Alternatively, an enriched problem can be considered, where the interface $\tilde{\Sigma}$ is obtained by considering an enlarged fine scale region $\tilde{\Omega}^{\mathrm{N}} \supset \Omega^{\mathrm{N}}$, see for instance [1]. If the *modeling error* is denoted by $(\boldsymbol{e}, \epsilon) = (\boldsymbol{u}_1 - \boldsymbol{u}_0, p_1 - p_0)$, the error in the goal can be stated exactly, as

Theorem 4. *(Error representation) In the case that* $(\boldsymbol{z}, \zeta)$ *is the exact dual solution, we have the error representation:*

$$J((\boldsymbol{u}_1, p_1)) - J((\boldsymbol{u}_0, p_0)) = \mathcal{R}((\boldsymbol{u}_0, p_0); (\boldsymbol{z}, \zeta)) + r,$$

with integral remainder term

$$\begin{aligned} r = -\int_0^1 \Big(& N''_{\Sigma_1}((\boldsymbol{u}_0 + s\boldsymbol{e}, p_0 + s\epsilon); (\boldsymbol{z}, \zeta), (\boldsymbol{e}, \epsilon), (\boldsymbol{e}, \epsilon)) + \\ & J''((\boldsymbol{u}_0 + s\boldsymbol{e}, p_0 + s\epsilon); (\boldsymbol{e}, \epsilon), (\boldsymbol{e}, \epsilon)) \Big)(1 - s) ds. \end{aligned}$$

Remark. The above result differs from [17] as the dual problem is the linearization of the fine-scale problem (20) rather than the mixed-model problem (22) as in [17].

Proof. (of theorem 4) Using appropriate Taylor expansions with integral remainders:

$$\begin{aligned} & J((\boldsymbol{u} + \boldsymbol{e}, p + \epsilon)) - J((\boldsymbol{u}, p)) = \\ & \quad J'((\boldsymbol{u}, p); (\boldsymbol{e}, \epsilon)) + \int_0^1 J''((\boldsymbol{u} + \boldsymbol{e}, p + \epsilon); (\boldsymbol{e}, \epsilon), (\boldsymbol{e}, \epsilon))(1 - s) ds \end{aligned} \tag{24a}$$

and

$$\begin{aligned} & N((\boldsymbol{u} + \boldsymbol{e}, p + \epsilon); (\boldsymbol{z}, \zeta)) - N((\boldsymbol{u}, p); (\boldsymbol{z}, \zeta)) = \\ & \quad N'((\boldsymbol{u}, p); (\boldsymbol{z}, \zeta), (\boldsymbol{e}, \epsilon)) + \\ & \quad \int_0^1 N''((\boldsymbol{u} + \boldsymbol{e}, p + \epsilon); (\boldsymbol{z}, \zeta), (\boldsymbol{e}, \epsilon), (\boldsymbol{e}, \epsilon))(1 - s) ds, \end{aligned} \tag{24b}$$

the error can be developed as

$$
\begin{aligned}
&J((\boldsymbol{u}_1,p_1)) - J((\boldsymbol{u}_0,p_0)) = \\
&\quad \overset{(24a)}{=} J'((\boldsymbol{u}_0,p_0);(\boldsymbol{e},\epsilon)) - \int_0^1 J''((\boldsymbol{u}+\boldsymbol{e},p+\epsilon);(\boldsymbol{e},\epsilon),(\boldsymbol{e},\epsilon))(1-s)ds \\
&\quad \overset{(23)}{=} N'_{\Sigma_1}((\boldsymbol{u}_0+s\boldsymbol{e},p_0+s\epsilon);(\boldsymbol{z},\zeta),(\boldsymbol{e},\epsilon)) - \\
&\qquad \int_0^1 J''((\boldsymbol{u}+\boldsymbol{e},p+\epsilon);(\boldsymbol{e},\epsilon),(\boldsymbol{e},\epsilon))(1-s)ds \\
&\quad \overset{(24a)}{=} N_{\Sigma_1}((\boldsymbol{u},p);(\boldsymbol{z},\zeta)) - N_{\Sigma_1}((\boldsymbol{u}_0,p_0);(\boldsymbol{z},\zeta)) - \\
&\qquad \int_0^1 \Big(N''_{\Sigma_1}((\boldsymbol{u}_0+s\boldsymbol{e},p_0+s\epsilon);(\boldsymbol{z},\zeta),(\boldsymbol{e},\epsilon),(\boldsymbol{e},\epsilon)) + \\
&\qquad J''((\boldsymbol{u}+\boldsymbol{e},p+\epsilon);(\boldsymbol{e},\epsilon),(\boldsymbol{e},\epsilon))\Big)(1-s)ds \\
&\quad \overset{(20-21)}{=} \mathcal{R}((\boldsymbol{u}_0,p_0);(\boldsymbol{z},\zeta)) + r,
\end{aligned}
$$

as required.

In the case under consideration, we have:

$$
\begin{aligned}
&\mathcal{R}((\boldsymbol{u}_0,p_0);(\boldsymbol{v},q)) = \\
&\qquad = (\boldsymbol{h},\boldsymbol{v})_{0,\partial\Omega_N} - a(\boldsymbol{u}_0,\boldsymbol{v}) - b(\boldsymbol{v},p_0) - b(\boldsymbol{u}_0,q) - c(\boldsymbol{u}_0,\boldsymbol{u}_0,\boldsymbol{v}) \\
&\qquad = -c^{\mathrm{S}}(\boldsymbol{u}_0,\boldsymbol{u}_0,\boldsymbol{v}) + F((\boldsymbol{v},q)) - N_{\Sigma_0}((\boldsymbol{u}_0,p_0);(\boldsymbol{v},q)) \\
&\qquad = -c^{\mathrm{S}}(\boldsymbol{u}_0,\boldsymbol{u}_0,\boldsymbol{v})
\end{aligned} \tag{25}
$$

In addition, we also have upper and lower bounds for the error estimate

Lemma 5. *For the case of a linear quantity of interest, and homogeneous Dirichlet boundary conditions ($\boldsymbol{u} = \boldsymbol{0}$ on $\partial\Omega$), the modeling error (4) is bounded as*

$$
|J((\boldsymbol{u}_1,p_1)) - J((\boldsymbol{u}_0,p_0)) - \mathcal{R}((\boldsymbol{u}_0,p_0);(\boldsymbol{z},\zeta))| \leqslant 2\sqrt{2}C_{\mathrm{PF}}\|\nabla\boldsymbol{z}\|_{0,\Omega}\|\nabla\boldsymbol{e}\|^2_{0,\Omega}, \tag{26}
$$

with C_{PF} the Poincaré-Friedrichs constant.

Proof. We have, for the second variation of N_{Σ_1}

$$
N''_{\Sigma_1}((\boldsymbol{u},p);(\boldsymbol{v},q),(\boldsymbol{w},r),(\boldsymbol{x},s)) = c(\boldsymbol{x},\boldsymbol{w},\boldsymbol{v}) + c(\boldsymbol{w},\boldsymbol{x},\boldsymbol{v}),
$$

and for the second variation of J, $J''(\cdot,\cdot,\cdot) = 0$. Substituting these relations into the error representation from theorem 4, yields

$$
J((\boldsymbol{u}_1,p_1)) - J((\boldsymbol{u}_0,p_0)) - \mathcal{R}((\boldsymbol{u}_0,p_0);(\boldsymbol{v},q)) = c(\boldsymbol{e},\boldsymbol{z},\boldsymbol{e}) + c(\boldsymbol{z},\boldsymbol{e},\boldsymbol{e})
$$

We invoke the continuity of the trilinear form, as given in e.g. [11, 15, 25]:

$$
|c(\boldsymbol{u},\boldsymbol{v},\boldsymbol{w})| \leqslant \sqrt{2}C_{\mathrm{PF}}\|\nabla\boldsymbol{u}\|_{0,\Omega}\|\nabla\boldsymbol{v}\|_{0,\Omega}\|\nabla\boldsymbol{w}\|_{0,\Omega} \qquad \forall \boldsymbol{u},\boldsymbol{v},\boldsymbol{w} \in V,
$$

where use has been made of a Ladyzhenskaya inequality [14] which, consistent with our definition of Ω in Section 2, is valid for subdomains of $\mathbb{R}^2$. We can thus bound the left member of (26) by $2\sqrt{2}C_{\mathrm{PF}}\|\nabla\boldsymbol{z}\|_{0,\Omega}\|\nabla\boldsymbol{e}\|^2_{0,\Omega}$ as asserted.

Remark. The bounds for nonlinear J depend on the type of nonlinearity and have to be assessed on a case-by-case basis. Note that the estimated error in the goal converges as $O(\|\nabla \boldsymbol{e}\|_{0,\Omega}^2)$, i.e., twice as fast as the modeling error in the norm. In the current case of mixed Stokes/Navier-Stokes approximations, the bounds on the estimate also converge as $O(\|\boldsymbol{e}\|_{0,\Omega}^2)$.

To elaborate the goal-adaptive procedure, we now consider a tessellation of the domains Ω^{N} and Ω^{S} into disjoint open sets (elements) $\kappa \in \mathcal{T}_h$ with a maximum diameter h. Constructed this way Σ does not dissect elements. The error can be split up into element contributions η_κ (indicators) such that

$$J((\boldsymbol{u}_1, p_1)) - J((\boldsymbol{u}_0, p_0)) \lesssim \textstyle\sum_{\kappa\in\mathcal{T}_h} \eta_\kappa, \tag{27}$$

with $\eta_\kappa \in \mathbb{R}$ a estimation of the local local contribution to the error at element κ. In the following we derive an error indicator η_κ that is designed to be convenient (viz., easily implemented and cheaply computed in standard finite element software), and moreover forms a sufficiently sharp upper bound for the error. We first make a few notes on discretization.

In practice, the primal problem (22) is approximated on finite dimensional conforming subspace $(\boldsymbol{u}_0^h, p_0^h) \in V^h \times Q^h \subset V \times Q$. In the context of the present work, we shall only consider modeling errors and assume that discretization errors are at least an order of magnitude smaller. For concurrent treatment of modeling and discretization errors, see [23, 24]. Then, the dual problem (23) may be solved in the same finite-dimensional subspace. The approximation space often consists of polynomial functions on each element $\kappa \in \mathcal{T}_h$. This space is spanned by a basis $\{\boldsymbol{\phi}_i\}_{i<N}$ with $\boldsymbol{\phi}_i : \Omega \to \mathbb{R}^3$, to each of which a unique point $\boldsymbol{x}_i \in \Omega$, a node, is assigned. Every basis function $\boldsymbol{\phi}_i$ maps to $\mathbb{R}^3$ as it has two velocity components and one pressure component.

Our goal now is to derive a simple error indicator η_κ, and our departure point is the nodal contributions to the dual-weighted residual. This approach is adopted as we work in the continuous Galerkin setting and the residual of the fine model $\mathcal{R}((\boldsymbol{u}_1, p_1); \cdot)$ is in general not orthogonal to element-wise restrictions of the dual $\boldsymbol{z}|_\kappa$, as these are not in the approximation space. On the other hand, the basis functions of course are, thus

$$\begin{aligned} J((\boldsymbol{u}_1, p_1)) - J((\boldsymbol{u}_0, p_0)) &= \mathcal{R}\left((\boldsymbol{u}_0, p_0); (\boldsymbol{z}, \zeta)\right) + r \\ &\approx \sum_{i<N} \underbrace{\mathcal{R}\left((\boldsymbol{u}_0, p_0); \boldsymbol{\phi}_i\right)}_{=:\hat{\mathcal{R}}_i} \hat{\boldsymbol{z}}_i \end{aligned}$$

where the hat denotes the i^{th} component of a function(al), and r the integral remainder term, which is assumed negligible. We note that on the discrete level, $\{\hat{\mathcal{R}}_i\}_i$ is just the residual vector, and $\{\hat{\boldsymbol{z}}_i\}_i$ contains the coefficients of the already computed dual solution. We define $I_\kappa := \{i < N : \boldsymbol{x}_i \in \bar{\kappa}\}$, the set of indices of nodes near element κ; and $\mathcal{T}_{h,i} := \{\kappa \in \mathcal{T}_h : \boldsymbol{x}_i \in \bar{\kappa}\}$, the set of elements near node $\boldsymbol{x}_i$. Recall that our goal is to define an element-wise rather than node-wise error indicator η_κ. This is because the indicators should inform the adaptation of the domain decomposition, which, like elements (unlike nodes), is a topological entity. We thus choose to redistribute contributions locally:

$$\mathcal{R}\left((\boldsymbol{u}_0, p_0); (\boldsymbol{z}, \zeta)\right) = \sum_{\kappa\in\mathcal{T}_h} \underbrace{\sum_{i\in I_\kappa} \overbrace{\frac{\int_\kappa \phi_i}{\int_\Omega \phi_i}}^{=:\beta_{i,\kappa}} \hat{\mathcal{R}}_i \hat{\boldsymbol{z}}_i}_{=:\eta_\kappa}.$$

The equality follows by the construction of $\beta_{i,\kappa}$ such that

$$\sum_{i<N} \alpha_i = \sum_{\kappa\in\mathcal{T}_h} \sum_{i\in I_\kappa} \beta_{i,\kappa} \alpha_i \tag{28}$$

for any real sequence $\{\alpha_i\}_{i<N}$. In the case of a non-uniform grid it may be hard to compute the integral of ϕ_i, as the elements in the support may be far from the node. This is because a basis function ϕ_i may have support on elements $\kappa \notin \mathcal{T}_{h,i}$ through constraints ensuring $C^0(\Omega)$-continuity of the basis. Information on the large support of such ϕ_i may not be readily available as the design philosophy of many finite element packages is to keep calculations local to elements. To handle such situations, we propose a simpler scheme, requiring only the local quantities $\mu(\kappa)$, the volume of the element; and $\#\mathcal{T}_{h,i}$, the number of elements neighboring node $\boldsymbol{x}_i$. We may approximate $\beta_{i,\kappa}$ by

1. splitting the contribution at i equally over the neighboring elements $\kappa \in \mathcal{T}_{h,i}$, i.e. $\dot{\beta}_{i,\kappa} = 1/\#\mathcal{T}_{h,i}$,
2. or slightly more refined, by splitting according to the element volumes, i.e. $\ddot{\beta}_{i,\kappa} = \mu(\kappa)/\mu(\cup_{\kappa\in\mathcal{T}_{h,i}}\kappa)$.

We denote the resulting approximate indicators by η^{c}_κ and η^{v}_κ, respectively. Note that $\dot{\beta}_{i,\kappa}$ and $\ddot{\beta}_{i,\kappa}$ satisfy the condition (28) so that we have the equalities

$$\mathcal{R}\left((\boldsymbol{u}_0, p_0); (\boldsymbol{z}, \zeta)\right) = \sum_{\kappa\in\mathcal{T}_h} \eta_\kappa = \sum_{\kappa\in\mathcal{T}_h} \eta^{\mathrm{c}}_\kappa = \sum_{\kappa\in\mathcal{T}_h} \eta^{\mathrm{v}}_\kappa$$

The final step is to select an algorithm for enhancing the model, i.e. updating Σ_0, based on the error indicators. Some common strategies are to refine those elements κ for which

1. $\eta_\kappa > \theta \max_\kappa \eta_\kappa$, with $0 \leqslant \theta \leqslant 1$ (greedy algorithm),
2. κ belongs to the fraction $0 < \theta \leqslant 1$ of elements with the largest indicator η_κ (fixed-fraction marking),
3. η_κ belongs to a minimal set of indicators such that their sum is at least $0 < \theta \leqslant 1$ of the total sum of indicators. This marking strategy is of the Dörfler type [6].

4. Numerical experiments

We investigate the flow in a channel with a cavity, the geometry of which is shown in Figure 2. It represents a square cavity hewn out of a channel side. The Reynolds number ($\mathrm{Re} := |\boldsymbol{v}|H/\nu$) is defined through the maximum inflow velocity $\max_{\partial\Omega_D} |\boldsymbol{g}|$, the sectional height H (which we both fix to unity) and kinematic viscosity ν. We consider only laminar flow and restrict the Reynolds numbers accordingly. The goal is to compute vorticity in the lower right corner of the cavity. Accordingly, $J((\boldsymbol{u}, p))$ is defined by (19). We prescribe the following boundary conditions

1. quadratic inflow profile: $\boldsymbol{g} = \{4y(1-y), 0\}$ at Γ_{in}, see Figure 2,
2. outflow boundary conditions: $\boldsymbol{h} = \boldsymbol{0}$ at Γ_{out},
3. no-slip boundary conditions: $\boldsymbol{g} = \boldsymbol{0}$ along the remainder of the boundary.

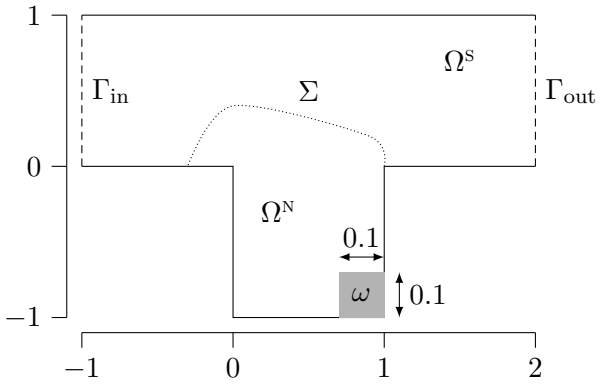

Figure 2: Schematic of cavity flow problem.

4.1. Discretization details

A uniform Cartesian mesh $\mathcal{T}_{h_0}$ is defined over the domain Ω, along with a set of uniform refinements $\mathcal{T}_{h_0/2^i}$, $i \in \mathbb{N}$. Also, an h-adapted grid $\mathcal{T}_0$ is generated, based on the fine model, Σ_1, with dual-weighted-residual-based indicators $\eta_\kappa := \|\mathcal{R}((\boldsymbol{u}_1, p_1), \cdot)\|_{0,\kappa} \|(\boldsymbol{z}, \zeta)\|_{0,\kappa}$, where the dual solution is calculated on a uniformly h-refined grid with a goal functional corresponding to that of the model adaptive simulation. The h-adapted mesh is introduced to ground the assumption that the modeling error is larger than the discretization error, as mentioned in Section 3. On this mesh we use the inf-sup stable, $\mathbb{Q}_2 - \mathbb{Q}_1$ Lagrange basis for $V^h \times Q^h$, see [4, 7].

The model-adaptive algorithm is outlined in table 1. The input Σ_0 is chosen such that $\Omega^{\mathrm{S}} = \Omega$, thus, we assume nothing about the location of the highest error contributions. The initial guess $(\boldsymbol{u}_0, p_0)$ is taken zero for low Reynolds numbers, and is obtained by Reynolds continuation for higher Reynolds numbers. Note that the adjoint problem and the error estimator can recycle many components of the primal problem, that is, the routine for assembling a residual vector and jacobian. We have also reused the `assembleResidual()` method for the error indicator, not just the convective term, as these are equivalent by (25). We have chosen in this schematic, and in our numerical investigations, to use the full model Σ_1 for the adjoint problem. The model refinement follows the greedy algorithm.

These computations were performed in the General Reacting Incompressible Navier-Stokes (GRINS) software package,which builds on `libMesh` [13].

4.2. $Re = 10$

We first consider the case Re = 10, on a uniform grid with 25600 elements ($h = 1/80$). Throughout we use the refinement fraction $\theta = 0.1$. In Figure (3), the error indicators; primal velocity magnitude and domain decomposition are plotted at successive model adaptive iterations i. Note that on a uniform grid $\eta_\kappa^{\mathrm{c}} = \eta_\kappa^{\mathrm{v}}$. The first plot, $i = 0$, is obtained using the full Stokes primal problem, before the governing equation is switched to the Navier-Stokes model on any element.

We observe that, of the competing error contributions, the two re-entrant corners dominate the error. This is due to the singularities in the pressure solution. The marked clefts in the error distribution that emanate from these corners become more pronounced under mesh refinement, and are related to a sign change in the indicator η_κ^{c}. We see that the error indicators are negligible inside the refined region, suggesting that the indicator indeed represents a local contribution to the error. This is as expected from the small support of the basis functions. In the coarse region, η_κ^{c} decreases on elements away from the interface, suggesting that a shape-gradient approach to

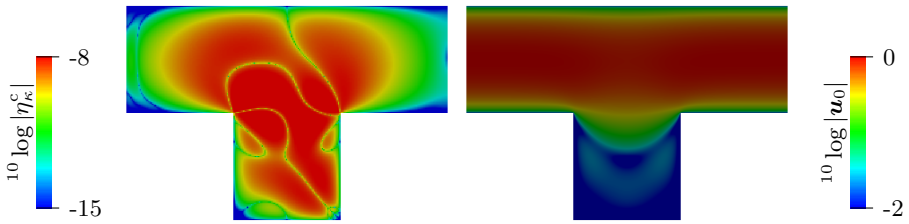

(a) $i = 0$, $\epsilon_Q = -4.12 \cdot 10^{-2}$, $\#\mathcal{T}_h^{\mathrm{N}}/\#\mathcal{T}_h = 0.000 = \mu(\Omega^{\mathrm{N}})/\mu(\Omega)$

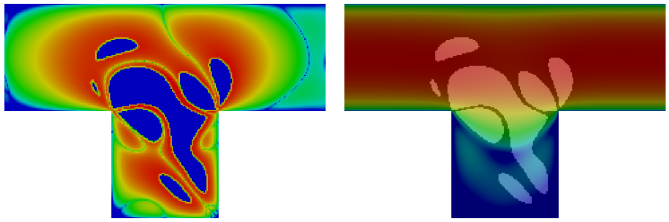

(b) $i = 1$, $\epsilon_Q = 4.43 \cdot 10^{-3}$, $\#\mathcal{T}_h^{\mathrm{N}}/\#\mathcal{T}_h = 0.195 = \mu(\Omega^{\mathrm{N}})/\mu(\Omega)$

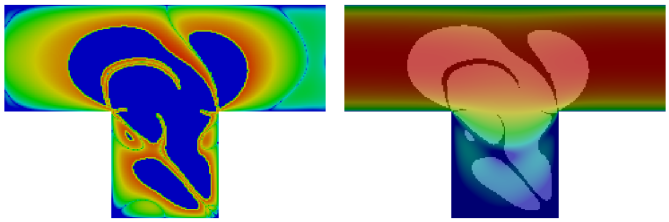

(c) $i = 2$, $\epsilon_Q = 2.12 \cdot 10^{-3}$, $\#\mathcal{T}_h^{\mathrm{N}}/\#\mathcal{T}_h = 0.392 = \mu(\Omega^{\mathrm{N}})/\mu(\Omega)$

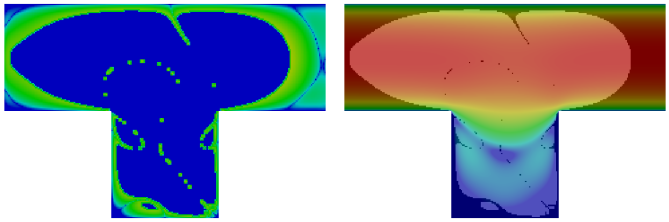

(d) $i = 4$, $\epsilon_Q = -2.56 \cdot 10^{-5}$, $\#\mathcal{T}_h^{\mathrm{N}}/\#\mathcal{T}_h = 0.743 = \mu(\Omega^{\mathrm{N}})/\mu(\Omega)$

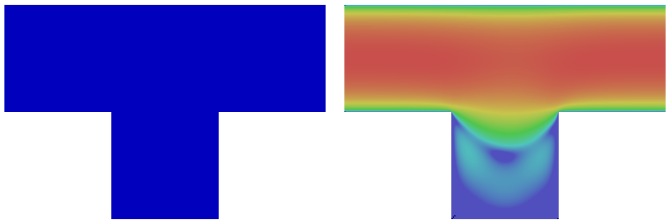

(e) $i = 13$, $\epsilon_Q = 1.08 \cdot 10^{-14}$, $\#\mathcal{T}_h^{\mathrm{N}}/\#\mathcal{T}_h = 1.000 = \mu(\Omega^{\mathrm{N}})/\mu(\Omega)$

Figure 3: Counting-based indicators η_κ^{c} (left) and primal velocity magnitude $|\boldsymbol{u}_0|$ (right) at model-adaptive step i for the case Re $= 10$, computed on a uniform mesh with resolution $h = 1/80$. The darker shading in the right-hand side plots indicates the Stokes domain. The relative error in the goal quantity is denoted by ϵ_Q, the fraction of refined elements by $\#\mathcal{T}_h^{\mathrm{N}}/\#\mathcal{T}_h$ and the volume fraction of the refined region by $\mu(\Omega^{\mathrm{N}})/\mu(\Omega)$.

Table 1: Pseudo code for the model-adaptive algorithm, given numerical parameters ($\texttt{TOL}_Q$ and θ) input Σ_0, Υ and initial guess $(\boldsymbol{u}_0, p_0)$.

```
do
  \\Solve forward problem
  R((u_0,p_0);·) = assembleResidual(Σ_0,Υ,(u_0,p_0),0)
  N'((u_0,p_0);·,·) = assembleJacobian(Σ_0,(u_0,p_0))
  (u_0,p_0) = solve(N'((u_0,p_0);·,·),R((u_0,p_0),·))

  \\Solve adjoint problem
  R((u_0,p_0);·) = assembleResidual(Σ_1,Υ_0,(u_0,p_0),Q'((u_0,p_0);·))
  N'((u_0,p_0);·,·) = assembleJacobian(Σ_1,(u_0,p_0))
  (z,ζ) = solve(N'((u_0,p_0);·,·)^T, R((u_0,p_0),·))

  \\Compute error,indicators and adaptively refine
  R((u_0,p_0);·) = assembleResidual(Σ_1,Υ,(u_0,p_0),0)
  {η_κ}_κ = computeIndicators(R((u_0,p_0);·),(z,ζ))
  Σ_0 = refineModel({η_κ}_κ,θ)
while |R((u_0,p_0),(z,ζ))| > TOL_Q
```

model adaptivity [2, 27] would also be interesting in this setting. In this approach, Σ is perturbed in the direction that yields an optimal error reduction. Furthermore, an approach with an enriched adjoint problem [1], where the interface is advanced uniformly to increase the fine region of the dual problem with respect to the primal problem, also looks promising. We also note that model refinement at the no-slip boundaries is postponed to the later iterations, due to the small values of the primal and dual velocities.

We now consider the same test case on a pre-computed h-adapted grid as plotted in Figure 4. Mesh refinement is concentrated around the reentrant corners and the integration region for the quantity of interest, and is thus seen to follow a different pattern than the model refinement. In Figures 5 and 6 we have plotted the model-adaptive iterations using indicators η_κ^{c} and η_κ^{v} respectively. Comparison reveals that the refinement patterns are very similar for the two indicators. We see roughly the same refinement patterns as for the uniform case of Figure 3, verifying that the indicators also work in the case of non-uniform meshes. The coarseness of the interface Σ is only a by-product of the lack of resolution. Note that the relative error in the quantity of interest is of equal order of magnitude for refinements of equal volume fraction $\mu(\Omega^{\mathrm{N}})/\mu(\Omega)$. However, the fraction of refined elements, $\#\mathcal{T}_h^{\mathrm{N}}/\#\mathcal{T}_h$, is 2-4 times lower than this volume fraction with both indicators. Thus, the chosen measure of computational expense does lead to different conclusions.

4.3. $Re = 1000$

At higher Reynolds numbers convection will play a more important role, especially in the cavity, where a stronger primary vortex forms and a larger secondary vortex entirely encapsulates ω, the goal quantity region. We immediately turn to the adaptive grid, shown in Figure 7. The h-refinement pattern is less concentrated and refines more along the wall of the domain.

We again plot error indicators and velocity magnitudes, in Figure 8. The high-valued errors are more localized and concentrated around the upstream pressure singularity and the primary vortex. These marked changes in refinement pattern should be ascribed to convection. Errors from

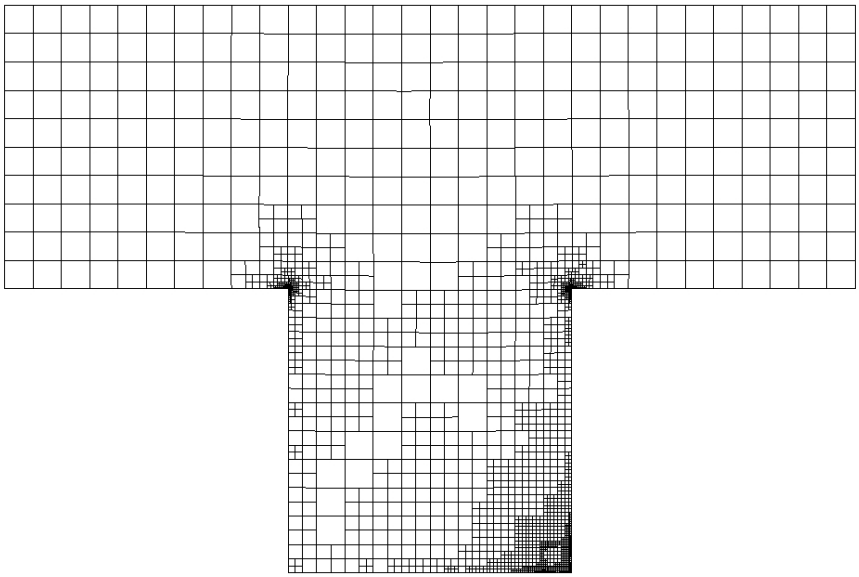

Figure 4: Pre-computed h-adapted mesh for the case Re = 10.

the upstream reentrant corner are convected to the primary vortex, of which the shape is highly dependent on the contribution of the convection term $c(\cdot,\cdot,\cdot)$. Model refinement is thus very much concentrated in the cavity, restoring quickly the parabolic profile inside the channel. This, in turn, renders Stokes flow a much better approximation to the flow (as the flow gradient is orthogonal to the flow direction, such that the convective term is small).

4.4. Effectivity and error decay

For the Reynolds numbers 10, 100 and 1000, we have also plotted the estimated relative error in the quantity of interest against the two different measures of cost: the fraction of fine elements $\#\mathcal{T}_h^{\mathrm{N}}/\#\mathcal{T}_h$ and the volume fraction of the fine region $\mu(\Omega^{\mathrm{N}})/\mu(\Omega)$, see Figure 10. As the Reynolds number increases, the error evolution becomes less smooth. Considerable model refinement is required to gain accuracy as the initial slope of the graphs is quite low, this is the case in the lower panel of Figure 10, where cost is measured in terms of the volume fraction. It would be more desirable to gain many orders of magnitude accuracy by refining a small part of the domain. This behavior is not observed due to the chosen test case, where the channel is relatively short. Note that the different indicators η_κ and their error bounds $\sum_\kappa |\eta_\kappa|$ perform approximately equally well. It can also be deduced that the model adaptive strategy shows how much refinement is necessary (i.e. what $\#\mathcal{T}_h^{\mathrm{N}}$ or $\mu(\Omega^{\mathrm{N}})$ is necessary) to get a certain level of accuracy. Mesh-independency is investigated in Figure 11, we see that the graphs corresponding to the same Reynolds numbers are indeed clustered, despite the low mesh resolution of the coarsest level.

In Figure 12, the effectivity of the estimator,

$$\theta_{\mathrm{eff}} = \frac{\mathcal{R}((\boldsymbol{u}_0, p_0); (\boldsymbol{z}, \zeta))}{J((\boldsymbol{u}_1, p_1)) - J((\boldsymbol{u}_0, p_0))}, \tag{29}$$

is plotted. We expect the effectivity to be close to unity as the errors in this estimate are $o(\|\boldsymbol{e}\|_{1,\Omega}^2 + \|\epsilon\|_{0,\Omega}^2)$ as shown in lemma 5. Errors are indeed small, especially at low Reynolds numbers, where the contribution of convection is relatively small. The evolution of the effectivity is rather erratic where the solution has not been resolved. This is because the error in primal velocity, $\boldsymbol{e}$ is still

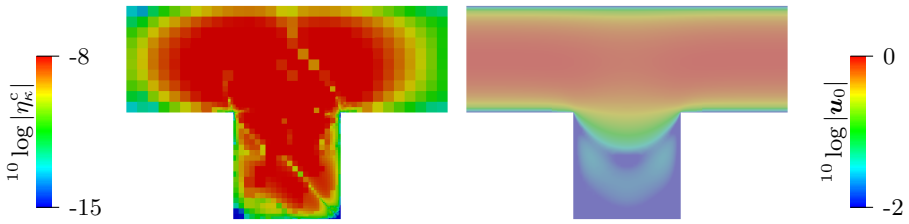

(a) $i = 0$, $\epsilon_Q = -4.11 \cdot 10^{-2}$, $\#\mathcal{T}_h^{\mathrm{N}}/\#\mathcal{T}_h = 0.000$, $\mu(\Omega^{\mathrm{N}})/\mu(\Omega) = 0.000$

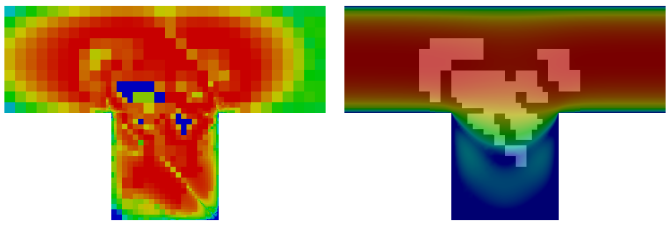

(b) $i = 1$, $\epsilon_Q = -3.26 \cdot 10^{-3}$, $\#\mathcal{T}_h^{\mathrm{N}}/\#\mathcal{T}_h = 0.044$, $\mu(\Omega^{\mathrm{N}})/\mu(\Omega) = 0.178$

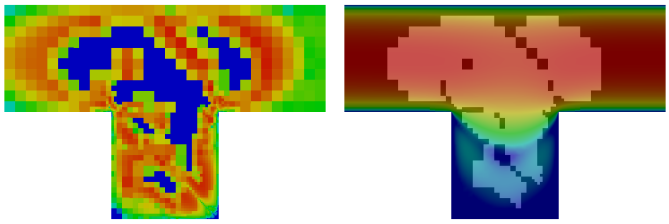

(c) $i = 2$, $\epsilon_Q = -1.35 \cdot 10^{-3}$, $\#\mathcal{T}_h^{\mathrm{N}}/\#\mathcal{T}_h = 0.130$, $\mu(\Omega^{\mathrm{N}})/\mu(\Omega) = 0.453$

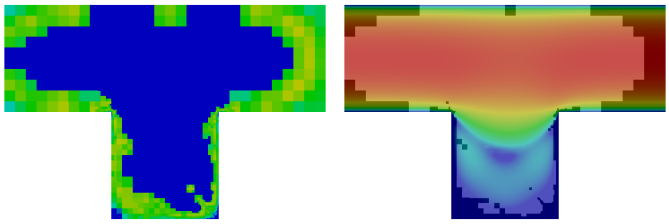

(d) $i = 4$, $\epsilon_Q = -6.32 \cdot 10^{-6}$, $\#\mathcal{T}_h^{\mathrm{N}}/\#\mathcal{T}_h = 0.362$, $\mu(\Omega^{\mathrm{N}})/\mu(\Omega) = 0.806$

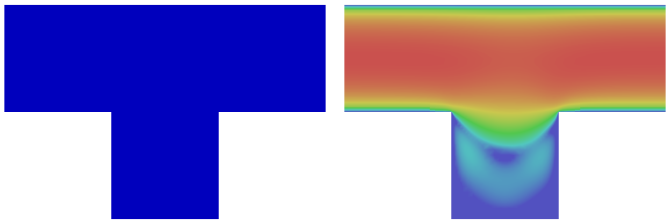

(e) $i = 12$, $\epsilon_Q = -5.93 \cdot 10^{-15}$, $\#\mathcal{T}_h^{\mathrm{N}}/\#\mathcal{T}_h = 0.986$, $\mu(\Omega^{\mathrm{N}})/\mu(\Omega) = 1.000$

Figure 5: Counting-based indicators η_κ^c (left) and primal velocity magnitude $|\boldsymbol{u}_0|$ (right) at model-adaptive step i for the case Re = 10, computed on the mesh of Figure 4. The darker shading in the right-hand side plots indicates the Stokes domain. The relative error in the goal quantity is denoted by ϵ_Q, the fraction of refined elements by $\#\mathcal{T}_h^{\mathrm{N}}/\#\mathcal{T}_h$ and the volume fraction of the refined region by $\mu(\Omega^{\mathrm{N}})/\mu(\Omega)$.

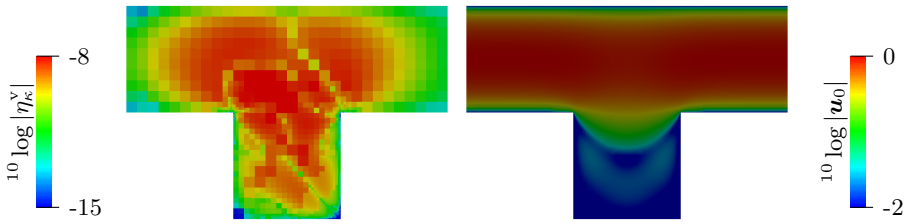

(a) $i = 0$, $\epsilon_Q = -4.11 \cdot 10^{-2}$, $\#\mathcal{T}_h^{\mathrm{N}}/\#\mathcal{T}_h = 0.000$, $\mu(\Omega^{\mathrm{N}})/\mu(\Omega) = 0.000$

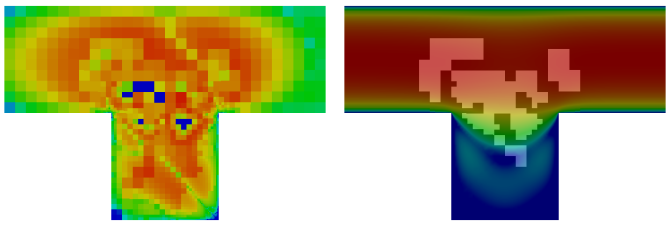

(b) $i = 1$, $\epsilon_Q = -5.59 \cdot 10^{-3}$, $\#\mathcal{T}_h^{\mathrm{N}}/\#\mathcal{T}_h = 0.041$, $\mu(\Omega^{\mathrm{N}})/\mu(\Omega) = 0.168$

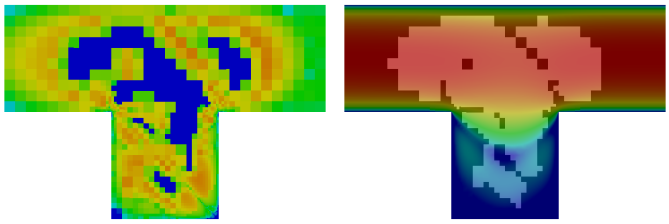

(c) $i = 2$, $\epsilon_Q = -1.96 \cdot 10^{-3}$, $\#\mathcal{T}_h^{\mathrm{N}}/\#\mathcal{T}_h = 0.119$, $\mu(\Omega^{\mathrm{N}})/\mu(\Omega) = 0.432$

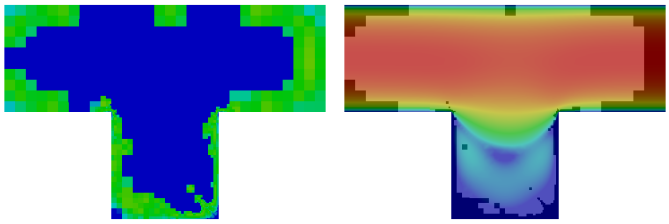

(d) $i = 4$, $\epsilon_Q = 1.01 \cdot 10^{-5}$, $\#\mathcal{T}_h^{\mathrm{N}}/\#\mathcal{T}_h = 0.379$, $\mu(\Omega^{\mathrm{N}})/\mu(\Omega) = 0.827$

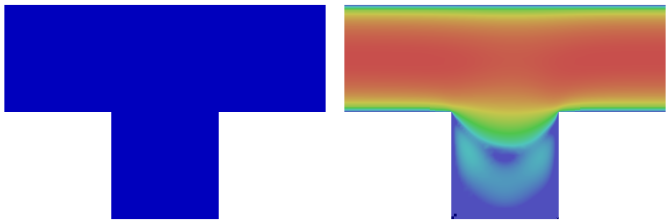

(e) $i = 12$, $\epsilon_Q = -2.21 \cdot 10^{-14}$, $\#\mathcal{T}_h^{\mathrm{N}}/\#\mathcal{T}_h = 0.985$, $\mu(\Omega^{\mathrm{N}})/\mu(\Omega) = 1.000$

Figure 6: Volume-based indicators η_κ^{v} (left) and primal velocity magnitude $|\boldsymbol{u}_0|$ (right) at model-adaptive step i for the case Re = 10, computed on the mesh of Figure 4. The darker shading in the right-hand side plots indicates the Stokes domain. The relative error in the goal quantity is denoted by ϵ_Q, the fraction of refined elements by $\#\mathcal{T}_h^{\mathrm{N}}/\#\mathcal{T}_h$ and the volume fraction of the refined region by $\mu(\Omega^{\mathrm{N}})/\mu(\Omega)$.

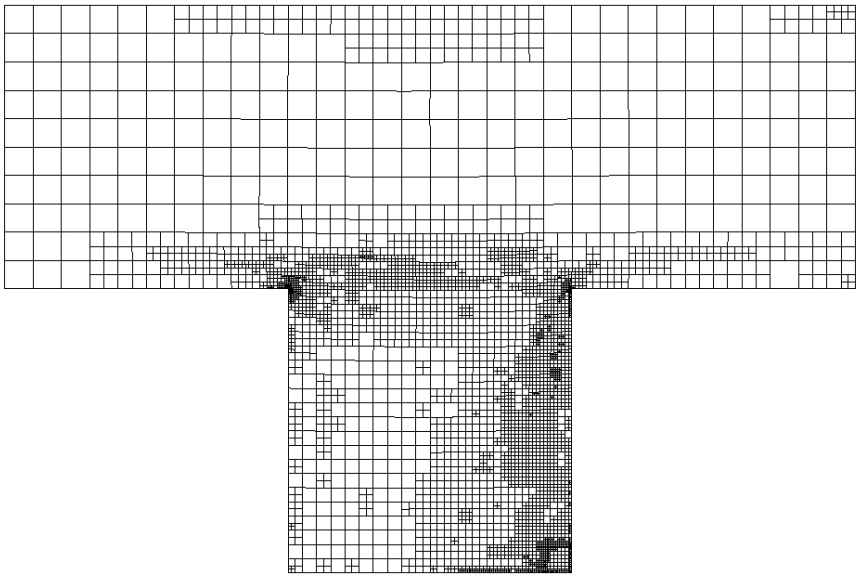

Figure 7: Adaptive mesh for the case Re = 1000 with $\#\mathcal{T}_0 = 4807$, $h = 1/10$ and 10 refinement levels.

large, hence, the integral remainder term in Theorem 4 is not negligible with respect to the dual weighted residual. Note that the effectivity becomes undefined when the fractions $\#\mathcal{T}_h^{\mathrm{N}}/\#\mathcal{T}_h$ and $\mu(\Omega^{\mathrm{N}})/\mu(\Omega)$ are exactly 1, where the limit to the exact solution is attained. Numerically, before this limit is attained, round-off errors start to dominate both the numerator and denominator of (29) already at $\#\mathcal{T}_h^{\mathrm{N}}/\#\mathcal{T}_h \gtrsim 0.95$ as observed in the upper panel of Figure 12.

5. Conclusions

We have presented two formulations for multi-model, viscous, incompressible, steady flow for the use in a model-adaptive scheme. A monolithic formulation was given and the derived partitioned formulation was proven to be equivalent. Simple but effective element-wise error indicator were presented, based on nodal components of the dual-weighted residual. Finally, a simple model-adaptive algorithm was presented where, at each iteration, first a forward problem is solved, an adjoint problem is solved, error indicators are computed and, finally, the model is locally refined.

The behavior of the error indicators and algorithm were demonstrated numerically for the monolithic formulation, for uniform as well as non-uniform grids. The developed technique automates the non-trivial process of domain decomposition, provides estimates (and bounds to the estimate) of the modeling error, and moreover offer insight into the flow features relevant to a specific quantity of interest. The refinement process behaves qualitatively the same on both h-adapted meshes and uniform meshes of different resolutions. Error indicators are seen to decrease smoothly in space, and monotonously (provided there is sufficient resolution) and suggest that adaptive approaches based on a shape-gradient approach, or an enriched adjoint solution would be effective in this context too.

6. Acknowledgments

This research is supported by the Dutch Technology Foundation STW, which is part of the Netherlands Organisation for Scientific Research (NWO) and partly funded by the Ministry of

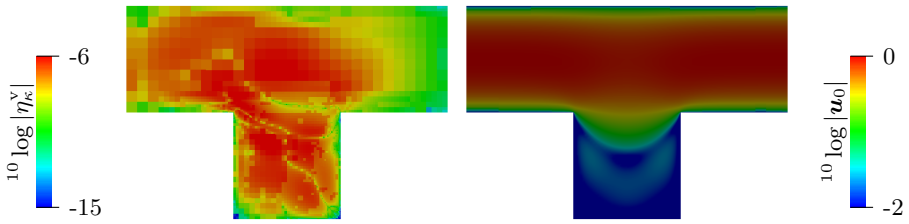

(a) $i = 0$, $\epsilon_Q = 1.73 \cdot 10^{0}$, $\#\mathcal{T}_h^{\mathrm{N}}/\#\mathcal{T}_h = 0.000$, $\mu(\Omega^{\mathrm{N}})/\mu(\Omega) = 0.000$

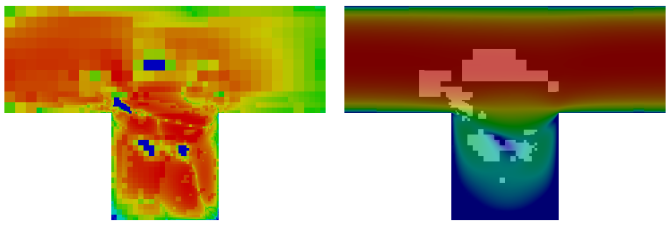

(b) $i = 1$, $\epsilon_Q = 1.42 \cdot 10^{0}$, $\#\mathcal{T}_h^{\mathrm{N}}/\#\mathcal{T}_h = 0.046$, $\mu(\Omega^{\mathrm{N}})/\mu(\Omega) = 0.103$

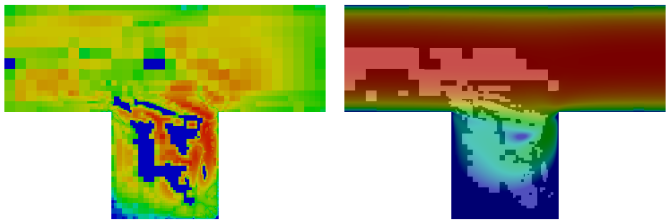

(c) $i = 2$, $\epsilon_Q = 7.86 \cdot 10^{-1}$, $\#\mathcal{T}_h^{\mathrm{N}}/\#\mathcal{T}_h = 0.193$, $\mu(\Omega^{\mathrm{N}})/\mu(\Omega) = 0.268$

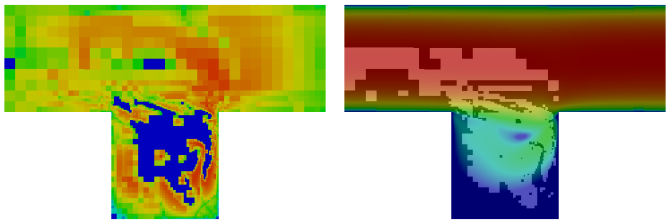

(d) $i = 3$, $\epsilon_Q = -1.48 \cdot 10^{0}$, $\#\mathcal{T}_h^{\mathrm{N}}/\#\mathcal{T}_h = 0.311$, $\mu(\Omega^{\mathrm{N}})/\mu(\Omega) = 0.301$

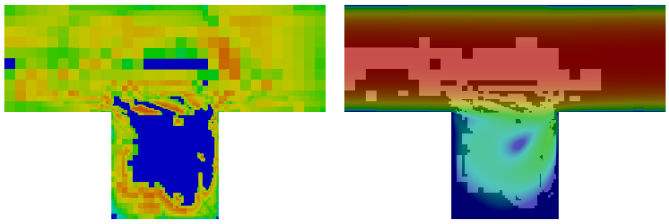

(e) $i = 4$, $\epsilon_Q = 4.04 \cdot 10^{-1}$, $\#\mathcal{T}_h^{\mathrm{N}}/\#\mathcal{T}_h = 0.424$, $\mu(\Omega^{\mathrm{N}})/\mu(\Omega) = 0.392$

Figure 8: Volume-based indicators η_κ^{v} (left) and primal velocity magnitude $|\boldsymbol{u}_0|$ (right) at model-adaptive step i for the case Re = 1000, computed on the mesh of Figure 7. The darker shading in the right-hand side plots indicates the Stokes domain. The relative error in the goal quantity is denoted by ϵ_Q, the fraction of refined elements by $\#\mathcal{T}_h^{\mathrm{N}}/\#\mathcal{T}_h$ and the volume fraction of the refined region by $\mu(\Omega^{\mathrm{N}})/\mu(\Omega)$. Continued in Figure 9.

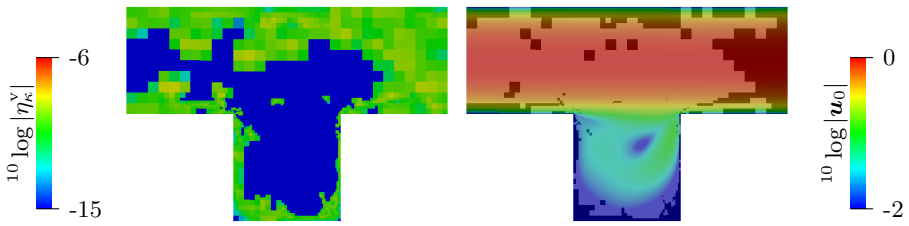

(a) $i = 7$, $\epsilon_Q = -1.26 \cdot 10^{-2}$, $\#\mathcal{T}_h^{\mathrm{N}}/\#\mathcal{T}_h = 0.698$, $\mu(\Omega^{\mathrm{N}})/\mu(\Omega) = 0.750$

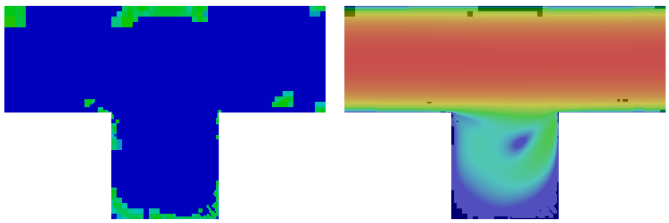

(b) $i = 10$, $\epsilon_Q = 1.44 \cdot 10^{-5}$, $\#\mathcal{T}_h^{\mathrm{N}}/\#\mathcal{T}_h = 0.861$, $\mu(\Omega^{\mathrm{N}})/\mu(\Omega) = 0.976$

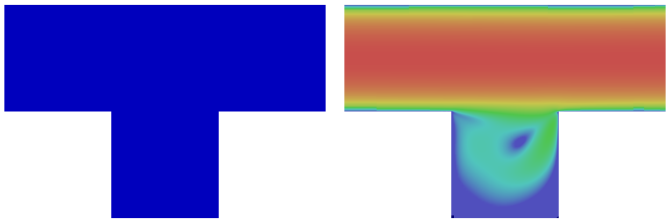

(c) $i = 16$, $\epsilon_Q = -1.85 \cdot 10^{-10}$, $\#\mathcal{T}_h^{\mathrm{N}}/\#\mathcal{T}_h = 0.996$, $\mu(\Omega^{\mathrm{N}})/\mu(\Omega) = 1.000$

Figure 9: Continuation of Figure 8.

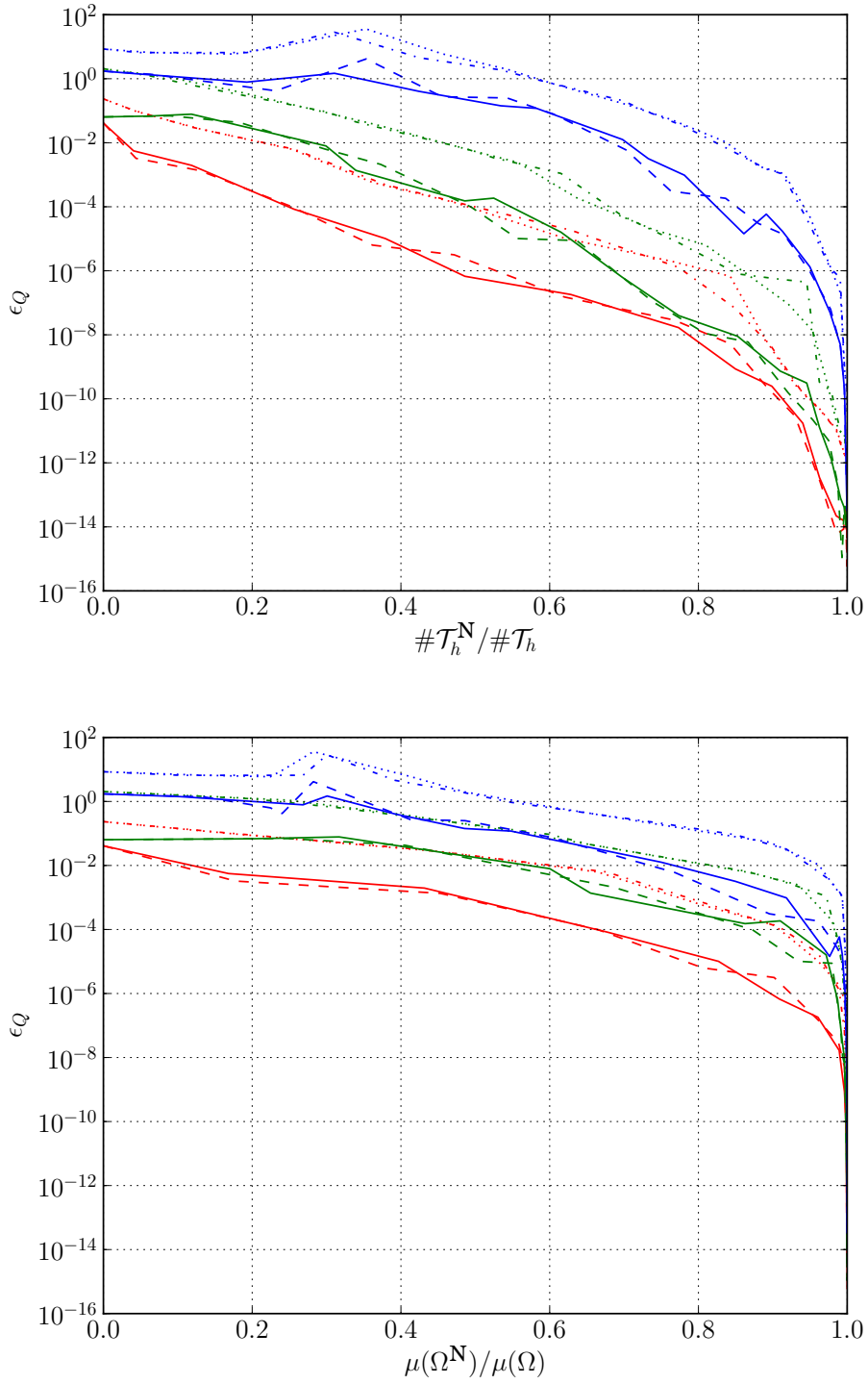

Figure 10: Error estimate for different estimators and Reynolds numbers, plotted against different measures for the cost. The line styles represent the simulation cases η_κ^{c} (−−) with error bound $\Sigma_\kappa|\eta_\kappa^{\mathrm{c}}|$ $(\cdots)$, and η_κ^{v} (—) with error bound $\Sigma_\kappa|\eta_\kappa^{\mathrm{v}}|$ $(-\cdot-)$. Colors represent different Reynolds numbers: Re = 10 (red), Re = 100 (green), Re = 1000 (blue).

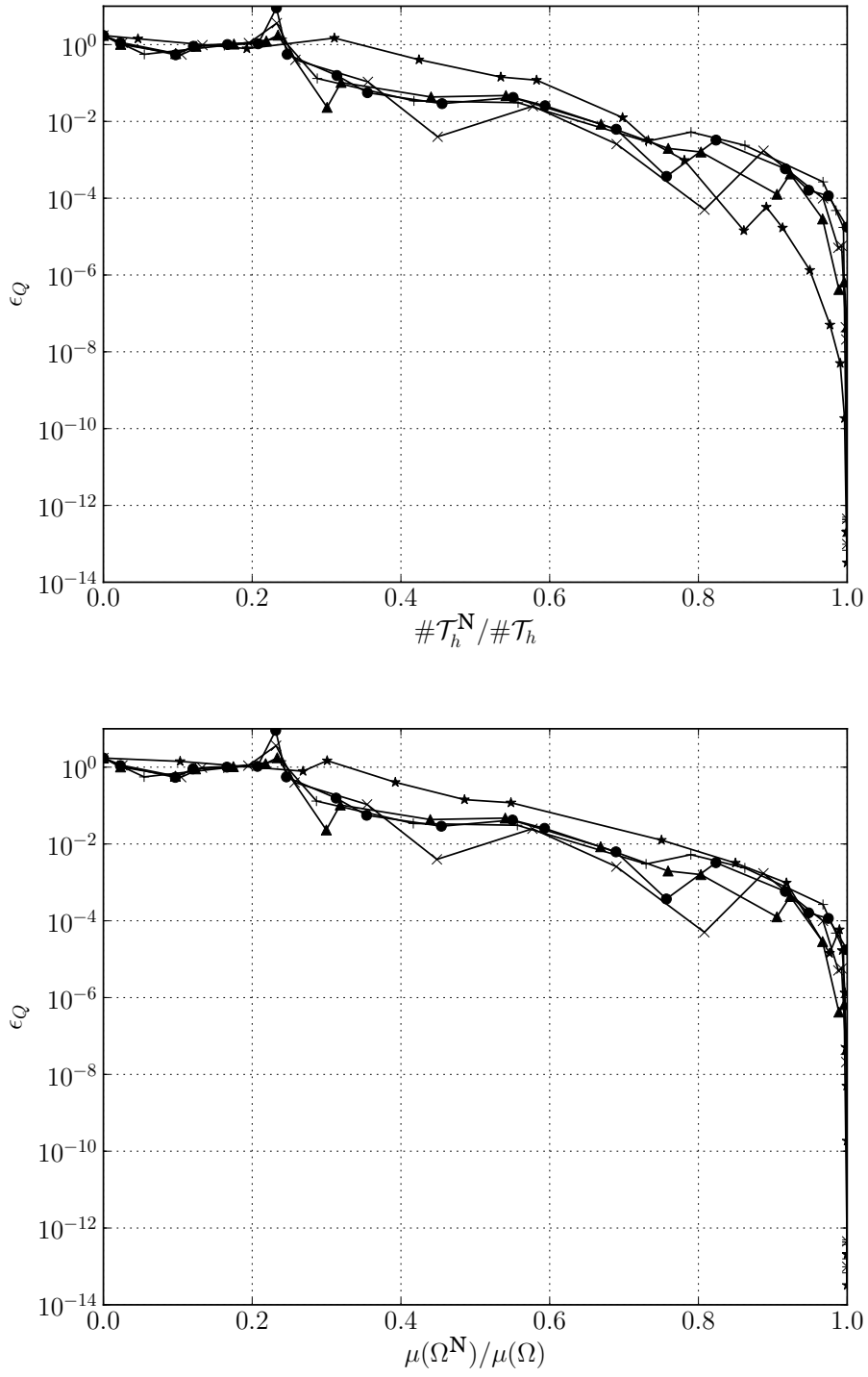

Figure 11: Error estimate for different meshes at $Re = 1000$. The line styles represent dierent mesh levels: $h = 1/10$ (+), $h = 1/20$ ($\times$), $h = 1/40$ ($\blacktriangle$), $h = 1/80$ ($\bullet$) and the mesh of Figure 7 ($\star$).

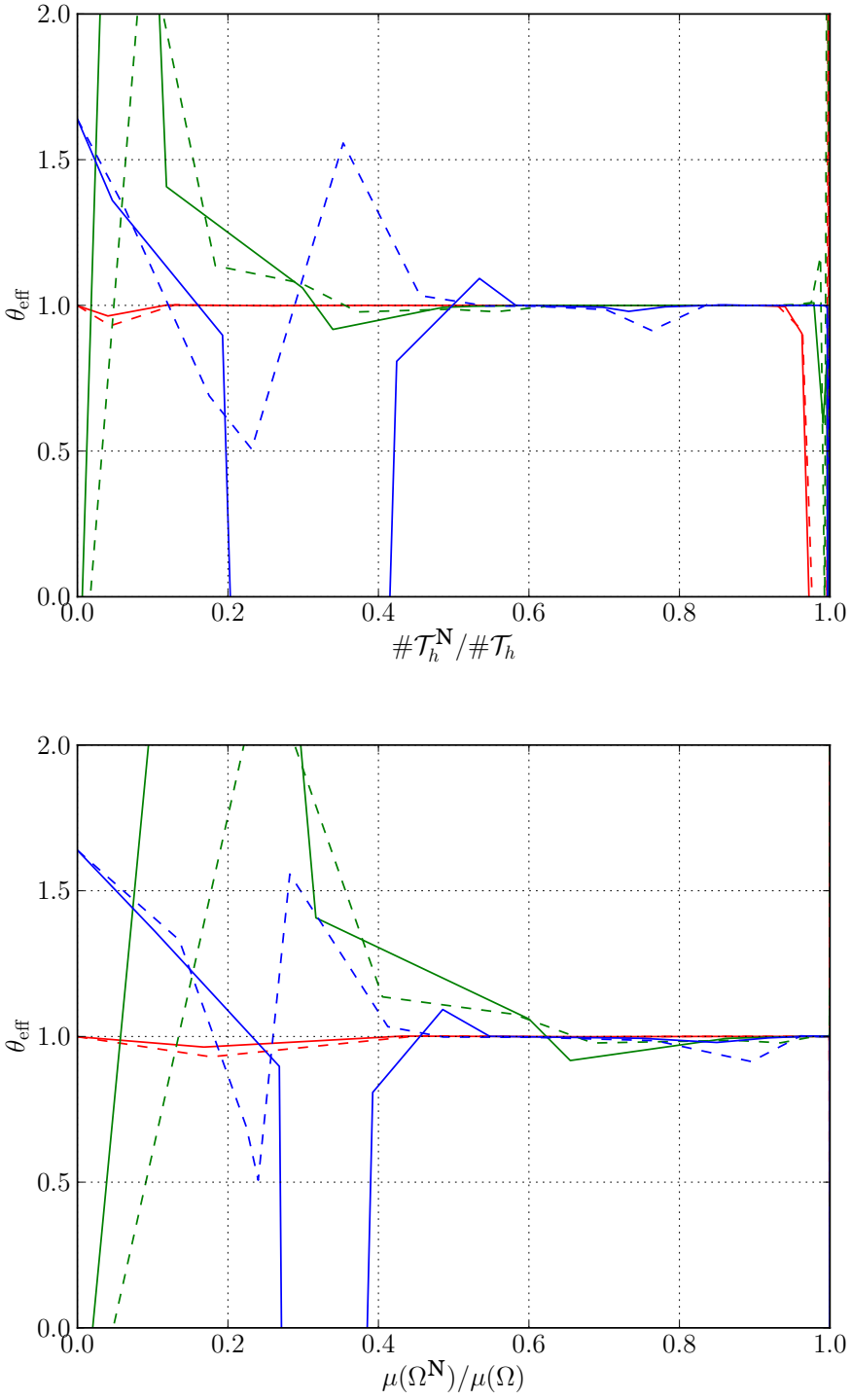

Figure 12: Effectivity of the error estimator for different uniform grids and Reynolds numbers. The line styles represent the simulation cases η_κ^{c} (−−) and η_κ^{v} (—). Colors represent different Reynolds numbers: Re = 10 (red), Re = 100 (green), Re = 1000 (blue).

Economic Affairs, Agriculture and Innovation (project number 10476). Paul T. Bauman was supported by the Department of Energy [National Nuclear Security Administration] under Award Number [DE-FC52-08NA28615]. Serge Prudhomme is a participant of the KAUST SRI Center for Uncertainty Quantification in Computational Science and Engineering.

References

[1] P.T. Bauman, J.T. Oden, and S. Prudhomme. Adaptive multiscale modeling of polymeric materials with arlequin coupling and goals algorithms. *Computer Methods in Applied Mechanics and Engineering*, 198(5–8):799–818, 2009.

[2] H. Ben Dhia, L. Chamoin, J.T. Oden, and S. Prudhomme. A new adaptive modeling strategy based on optimal control for atomic-to-continuum coupling simulations. *Computational Methods in Applied Mechanics and Engineering*, 200:2675–2696, 2011.

[3] M. Braack and A. Ern. A posteriori control of modeling errors and discretization errors. *Multiscale Modeling and Simulation*, 1(2):221–238, 2003.

[4] F. Brezzi and R. Falk. Stability of higher-order hood–taylor methods. *SIAM Journal on Numerical Analysis*, 28(3):581–590, 1991.

[5] C. Carstensen, S.A. Funken, and E.P. Stephan. On the adaptive coupling of FEM and BEM in 2D elasticity. *Numerische Mathematik*, 77:187–221, 1997.

[6] W. Dörfler. A convergent adaptive algorithm for Poisson's equation. *SIAM Journal on Numerical Analysis*, 30:1106–1124, 1996.

[7] A. Ern and J. L. Guermond. *Theory and Practice of Finite Elements*. Applied Mathematical Sciences. Springer, 2004.

[8] A. Ern, S. Perotto, and A. Veneziani. Hierarchical model reduction for advection-diffusion-reaction problems. In Karl Kunisch, Günther Of, and Olaf Steinbach, editors, *Numerical Mathematics and Advanced Applications*, pages 703–710. Springer Berlin Heidelberg, 2008.

[9] L. Fatone, P. Gervasio, and A. Quarteroni. Multimodels for incompressible flows. *Journal of Mathematical Fluid Mechanics*, 2:126–150, 2000.

[10] L. Fatone, P. Gervasio, and A. Quarteroni. Multimodels for incompressible flows: iterative solutions for the navier-stokes/oseen coupling. *Mathematical Modelling and Numerical Analysis*, 35(3):549–574, 2001.

[11] G.P. Galdi. *An Introduction to the Mathematical Theory of the Navier-Stokes Equations*. Springer Monographs in Mathematics. Springer, 2nd edition, 2011.

[12] J. Hoffman, J. Jansson, and R. V. De Abreu. Adaptive modeling of turbulent flow with residual based turbulent kinetic energy dissipation. *Computer Methods in Applied Mechanics and Engineering*, 200(37-40):2758–2767, 2011. Special Issue on Modeling Error Estimation and Adaptive Modeling.

[13] B.S. Kirk, J.W. Peterson, R.H. Stogner, and G.F. Carey. `libMesh`: A C++ Library for Parallel Adaptive Mesh Refinement/Coarsening Simulations. *Engineering with Computers*, 22(3–4):237–254, 2006.

[14] O.A. Ladyzhenskaya. *The Mathematical Theory of Viscous Incompressible Flows*. Mathematics and its Applications. Gordon and Breach, revised english edition, 1963.

[15] W.J. Layton. *Introduction to the Numerical Analysis of Incompressible Viscous Flows*. SIAM, Philadelphia, 2008.

[16] W.C.H. McLean. *Strongly Elliptic Systems and Boundary Integral Equations*. Cambridge University Press, 2000.

[17] J.T. Oden and S. Prudhomme. Estimation of modeling error in computational mechanics. *Journal of Computational Physics*, 182:496–515, 2002.

[18] J.T. Oden and K.S. Vemaganti. Estimation of local modeling error and goal-oriented adaptive modeling of heterogeneous materials. *Journal of Computational Physics*, 164:22–47, 2000.

[19] S. Perotto. Adaptive modeling for free-surface flows. *ESAIM Mathematical Modelling and Numerical Analysis*, 40(3):469–499, 2006.

[20] S. Prudhomme, H. Ben Dhia, P.T. Bauman, N. Elkhodja, and J.T. Oden. Computational analysis of modeling error for the coupling of particle and continuum models by the arlequin method. *Computer Methods in Applied Mechanics and Engineering*, 197(41–42):3399—3409, 2008.

[21] S. Prudhomme and J.T. Oden. Computable error estimators and adaptive techniques for fluid flow problems. In *Lecture Notes in Computational Science and Engineering*, volume 25, pages 207–268. Springer-Verlag, 2002.

[22] C. Schwab. *$p-$ and $hp-$ Finite Element Methods*. Oxford Science Publications, Oxford, 1998.

[23] E. Stein and M. Rüter. *Encyclopedia of Computational Mechanics*, volume 2 Structures, chapter 2 Finite Element Methods for Elasticity with Error-controlled Discretization and Model Adaptivity, pages 5–58. Wiley, 2004.

[24] E. Stein, M. Rüter, and S. Ohnimus. Implicit upper bound error estimates for combined expansive model and discretization adaptivity. *Computer Methods in Applied Mechanics and Engineering*, 200(37-40):2626–2638, 2011. Special Issue on Modeling Error Estimation and Adaptive Modeling.

[25] R. Temam. *Navier-Stokes equations: Theory and Numerical Analysis*. North-Holland, Amsterdam, 1977.

[26] E.H. van Brummelen, K.G. van der Zee, V.V. Garg, and S. Prudhomme. Flux evaluation in primal and dual boundary-coupled problems. *Journal of Applied Mechanics*, 79(010904-1), 2012.

[27] K.G. van der Zee, S. Prudhomme, and J.T. Oden. Adaptive modeling for partitioned-domain concurrent multiscale models: A posteriori estimates and shape-derivative strategies for continuum models. Technical Report To appear, ICES, 2013.

[28] K.G. van der Zee, E.H. van Brummelen, I. Akkerman, and R. de Borst. Goal-oriented error estimation and adaptivity for fluid–structure interaction using exact linearized adjoints. *Computer Methods in Applied Mechanics and Engineering*, 200(37-40):2738–2757, 2011. Special Issue on Modeling Error Estimation and Adaptive Modeling.

[29] T.M. van Opstal and E.H. van Brummelen. A potential boundary element method for large-displacement fluid-structure interaction. *Computer Methods in Applied Mechanics and Engineering*, page (submitted), 2013.

[30] T.M. van Opstal, E.H. van Brummelen, R. de Borst, and M.R. Lewis. A finite-element/boundary-element method for large-displacement fluid-structure interaction. *Computational Mechanics*, 50(6):779–788, 2012.

[31] O.C. Zienkiewicz, D.W. Kelly, and P. Bettess. *Marriage* à la mode–*The Best of Both Worlds (Finite Elements and Boundary Integrals)*, pages 59–80. Wiley, 1979.